Universitat Politècnica de Catalunya
Departament de Física Aplicada

Nonlinear one-zone models of stellar pulsations

by

Andreea Munteanu

A thesis submitted for the degree of

Doctor of Philosophy

Advisors:
Prof. Enrique García–Berro
Prof. Jordi José

Barcelona, December 2003

To my parents who fostered my curiosity about how nature works

Acknowledgements

I would like to acknowledge and express gratitude to those numerous people that have supported, encouraged and nudged me through the thesis process. Regrettably, but inevitably, the following list of names will be incomplete, and I hope that those who are missing will forgive me, and will still accept my sincere appreciation of their influence on my work.

I cannot start these acknowledgements in another way but by recognizing the immense contribution that my family has made to my choice of starting this work. Despite living far away, they are constantly in my thoughts and their love and support have been a major stabilizing force over these past three years. I thank my father for teaching me to ask myself the most thought-provoking questions and to my mother, from whom I've learned that every challenge one takes becomes a victory if embraced with confidence, patience, serenity and especially joy. Their unquestioning faith in me and in my abilities has helped to make all this possible. For that, for being my model of unflagging dedication to a goal and for owing what I am entirely to them, I dedicate this thesis to my parents.

Pursuing a Ph.D. research within a research group whose main focus differs to some degree from that of the work described in this thesis has been a great challenge. The person accepting the challenge was not I, but my advisor, Enrique García–Berro and thus my highest gratitude goes to him for accepting me as a postgraduate student, for agreeing on my choice of topic and for letting me have the just-right measure of freedom. I must thank him for believing in me before I believed in myself and for his constant reassurance that steep hills must be climbed one step at a time, which always reminded me of a phrase in a favorite movie of mine saying "Small moves, Ellie, small moves!". He also epitomizes the word "meticulous" when it comes to figures and documents styles. I have to say that in this field the pupil finally outdid the master, and I thank the master for tolerating my exaggerated perfectionism of the last few months. In the same spirit, I must thank my second advisor, Jordi José to whom this thesis also owes its existence. He always found words of encouragement and support, and especially time to read through numerous (and sometimes premature) draft manuscripts with incredible patience and dedication, finding errors or misplacements when it was highly improbable that any still existed.

My years at UPC have had an intensity which I may miss many years from now. The people here, however, I will miss as soon as this work is finished. I am thankful

that almost every person I have met here has made my stay significantly more enjoyable. I have to acknowledge my office mates Pilar Gil, Santiago Torres and Pablo Loren for being such entertaining coworkers and for the successful team-work we have done in keeping each other sane in front of the spooky and random behavior of the computers in moments of crisis. A big THANK YOU goes to Pilar for offering her help on the slightest notice of trouble and for caring always more about the others than about herself. I owe to her patience and perseverance the wonderful flat I lived in for more than two years. Particularly, I am very obliged to her for patiently checking every official document I wrote in Spanish in search for missing accents and invented words. During these years within the astrophysics community at UPC, I have particularly enjoyed the seminars at IEEC which have permanently reminded me of how wonderful, inspiring and surprising the universe is and of the immeasurable number of mysteries still to be untangled.

I wish to acknowledge the invaluable contribution of Emilia Petrişor who initiated me in the field of nontwist maps with inexhaustible patience and whose prompt replies to all my mathematical questions and troubles have contributed undoubtedly and crucially to the present thesis. Within the same field, I thank Amadeu Delshams and Tere Seara for clearing in several occasions many of my doubts in this field. Similarly, I am grateful to Giuseppe Bono for the endless phone-talks about stellar convection, for his kind welcome at the Observatory of Rome and from whom I have learned that science and research are not only about discovering and inventing, but mainly about discerning what you think you know from what you really know.

Many parties, lunches, dinners and moments of despair were shared with the other PhD students from this department. Cesca Ribes and Yolanda Ciriano have been invaluable references for the warmest hospitality as well as for providing advice, friendship and for the many therapeutic discussions with or without a cup of coffee. Alejandro Carrillo has been an inspiring friend for all of us for his joyful and positive character, for his sincere compliments and unintelligible jokes and for being the unlimited provider of Bailey's for Friday's "café con Bailey's". The ironic and provoking jokes of David Pino have created the necessity for my accelerated learning of the Spanish language and I found that extremely useful and stimulating. Undoubtedly, the last two years would have been incomparably prosaic were not for the members of the Complex Systems Group. The time spent with them over various transcendental and sublunary conversations as well as in the never-ending haywire jokes-contest is priceless and has definitely helped in awakening my dormant resilient side. For this, for witnessing an active team-work and for all the wonderful thinks I have learned being near them, I highly admire them all. Jordi Delgado has always been a source of enthusiasm and endless jokes, and due to his vivid interest for "misbehaved" pulsating stars, he has been an important source of books and articles. An invaluable provider of books, articles and support has been all these years Ricard Solé, the perfect model of the unconventional scientist whose brilliance, wit and lectures I have found highly inspiring. By the way, I hope to attend more of his seminars or talks in the future and that one of these be on graphs or brain dynamics!

I also wish to acknowledge the whole staff of the Department of Applied Physics for their dedication in creating a pleasant and stimulating working environment. Silvia Soriano, Rosa Maria Laina and Àngel Andres are worthy of special thanks for their priceless help and promptness in matters requiring secretarial skills and for having the right answer to all the possible questions and problems I addressed them. The present and past computer-support-crew — Amador Álvarez, Josep Sanz and Fernando Verdugo — has courageously survived the bombardment of simple and complex problems to which all the PhD students have exposed them and deserve special thanks.

Unconventionally, perhaps, I would also like to thank myself. I have had two Andreea's inside my head for the past six months: the pessimistic one saying that I cannot possibly finish it in such a short time and that it's not worth it, and the optimistic one standing serenely in front of me every single day just holding up a big list entitled "Reasons Why You Choose To Do This". I have done it because I wanted to do it and because I have enjoyed every minute of it.

And I have saved the best for last and the best is Pau, the person who completely changed my life in the last two years, who is undeniably the cause of my happiness and who has helped substantially the latter Andreea in adding items to her optimistic list. Firstly, I thank him for the best gift of all, that of learning. He taught me to take the slightest problem or caprice as a challenge and learn from all the steps to its solving. From him, I've learned to look always for improvements, up to the highest unthinkable level of perfectionism, to avoid at any cost the routine (by means of routines and subroutines) and to make of every day a world to discover despite any obstacle. Finally, I thank him for his unfailing support and inexhaustible optimism, for helping me keep things in perspective, for the numerous conversations that have shaped my horizon (more to come, hopefully) and for giving me inconceivably more than I desired. In the same direction, a big hug and my most sincere gratitude go to the entire Quer, Fernández and Duran families for cuddling me so much.

Science is a noble pursuit, and those who pursue it have given their lives to a worthy cause. Nobles, alea jacta est!

Desde un punto de vista material, esta tesis ha sido realizada gracias a la beca de la Agencia Española de Cooperación Internacional del Ministerio de Asuntos Exteriores. Y gracias a los esfuerzos continuos y tenaces de Enrique como organizador y redactor, he podido participar, junto con otros miembros de nuestro grupo de Astronomía y Astrofísica en los siguientes proyectos:

- DGES, Promoción General del Conocimiento, Objetos compactos, explosiones estelares y sus implicaciones cosmológicas, PB98–1183–C03–02;
- MCYT, Plan Nacional de Astronomía, Estados avanzados de la Evolución Estelar: Teoría y Aplicaciones a Escala Galáctica, AYA2000-1785;
- MCYT, Plan Nacional de Astronomía, La población de enanas blancas en el halo galáctico, AYA2002-04094-C03-01;
- MCYT/Max Planck Gesellschaft, Acción Integrada Hispano–Alemana, La función de luminosidad de las enanas blancas como trazadora de la evolución de la Galaxia, HA2000–0038.

"The main role of models is not so much to explain and to predict — though ultimately these are the main functions of science — as to polarize thinking and to pose sharp questions. Above all, they are fun to invent and to play with, and they have a life of their own. The "survival of the fittest" applies to models even more than it does to leaving creatures. They should not, however, be allowed to multiply indiscriminately without real necessity or real purpose."

Mark Kac
Science **166**, 695 (1969)

Contents

Motivation and outline of the thesis

Variable stars are stars that vary in their light output. The origin of this variability may be intrinsic, in which the variability is either of pulsating type or of eruptive type, while the extrinsic variability leads to two other classes of variable stars: eclipsing binaries and rotating stars. We started on the quest that led to this thesis work with a lot of enthusiasm and curiosity for finding out what is the mechanism that drives irregularly pulsating stars. The large-amplitude long-period variables generally called Mira variables were the first to attract the attention of many astronomers — see the historical introduction of Gautschy (1997). David Fabricius mentioned the variability of o Ceti, the prototype of Mira variables, in 1596 in a letter to Tycho Brahe. Significantly later, more precisely in 1784, John Goodricke discovered the variability of δ Cephei, the second known Cepheid variable and name patron for this very important class of variable stars. In the absence of any other viable theory on the cause of this stellar variability, the pulsating stars were interpreted as binaries until the beginning of the 20^{th} century. Even if some ideas on intrinsic variability started to appear at the end of the 19^{th} century, it is only in the mid-sixties that computational studies (Baker & Kippenhahn 1962) replaced manual discretization and calculus and brought the final explanation of the Cepheid-type pulsational instability, as it will be shortly exposed in the Introduction. Ever since, astrophysicists have concentrated their efforts on the regular classical variables for which most of the basic pulsation mechanism is now understood. Semiregular and irregular variables and some Mira-type variables which exhibit erratic or strange behavior have been generally disregarded until recently. This was mainly due to the lack of high-accuracy data and perhaps to an apparent lawless and stochastic behavior. With the advent of the rapid developments in nonlinear time-series analysis and in the theory of dynamic systems with emphasis on chaotic dynamics, the study of the irregular variability has become a hot topic. Mainly due to pioneers such as J. Robert Buchler, Jean Perdang and Edward A. Spiegel (Buchler et al. 1985), irregular stellar variability proved to be, in some cases, due to deterministic chaos, and nonlinear phenomena in stellar astrophysics turned into a research field of its own (Takeuti & Buchler 1993).

In this context and in the framework of the theory of nonlinear dynamics in which simple models can exhibit complex behavior, we have engaged in this endeavor of seeking for the root-cause of the complex stellar variability by means of simple models. The main questions leading us in our work were:

1. Why do some stars pulsate irregularly?
2. Is irregularity a common evolutionary phase in evolved stars?
3. What evolutionary consequences can the irregular pulsations have on the life of the star?
4. What are the consequences of the interplay between pulsation and convection?
5. What feedback exists between pulsation and mass loss?
6. What can or cannot one-zone models account for and which are their limitations?

Even if some of the above questions will not be commented throughout this thesis, they served their role as guiding lights and helped us in interpreting our results.

As a natural sequence of this section, we introduce in Chapter 1 more details about the main causes of intrinsic stellar variability and present some of the basic equations of stellar pulsations that are used frequently throughout this thesis. In Chapter 2, we review the most relevant simple models and the models which played an important role in our approach to studying stellar pulsations. Chapter 3 concerns a simple oscillator proposed and studied in Icke et al. (1992) which is aimed to reproduce the adiabatic radial pulsations of small and intermediate mass stars ($M \leq 8M_{\odot}$) exhibiting pulsational instability when reaching the evolutionary phase called the Asymptotic Giant Branch (AGB). We present the results obtained by analyzing this model extended to characterize more massive and luminous stars ($8M_{\odot} \leq M \leq 11M_{\odot}$). We expose in detail the outcome of the parametric study with emphasis on the local and global bifurcations undergone by the dynamic system and their influence on the subsequent behavior. This work was included in a series of articles of a slightly more mathematical nature than the present astrophysical thesis, and therefore only the basic mathematical results appear in the present thesis. However, the reader is referred to the corresponding bibliography for more mathematical implications of the dynamics. In Chapter 4, we introduce a one-zone model of nonlinear nonadiabatic stellar oscillations. We present the parametric study of the system and draw attention on a particular set of numerical solutions which may have implications in the study of the variability of long period variables. In Chapter 5, we investigate the pulsation-convection interaction in the framework of the nonadiabatic one-zone model proposed in Stellingwerf (1986). We present comments and caveats on the results from this model as they appear in several papers in the relevant literature, and we also introduce new results and further possible extensions of the model. Finally, we conclude the work exposed in the previous chapters and discuss the questions that this study has raised, that are more numerous, as is often the case, than the questions initially asked.

Chapter 1

Introduction

The study of pulsating stars has attracted much attention from astronomers. Pulsational instabilities are encountered in many phases of stellar evolution, and also for a wide range of stellar masses. Moreover, pulsational instabilities provide a unique opportunity to learn about the physics of stars and to derive useful constraints on the stellar physical mechanisms that would not be accessible otherwise (see Stobie & Whitelock 1995).

1.1 Important timescales

Before discussing the stability and the dynamics of stellar structure, we shall consider, for orientative purposes, some important timescales and their corresponding orders of magnitude. They are of particular interest in connection with the study of pulsating stars. The first one of these is the free-fall or dynamic timescale, $t_{\rm ff}$ which is the characteristic time associated with a dynamic collapse. When evolutionary times approach the free-fall timescale significant departures from hydrostatic equilibrium are expected. An estimate of the order of magnitude can be readily obtained by calculating the time required for a unit mass to fall freely through a distance of the order of $R_\star$ (the stellar radius) under the influence of a (constant) gravitational acceleration equal to the surface gravity $GM/R_\star^2$ of a star of mass M:

$$t_{\rm ff} \sim \frac{1}{\sqrt{G\,\overline{\rho}}}, \tag{1.1}$$

where $\overline{\rho}$ is the average density. It will be seen later that the pulsation periods are comparable to this timescale. This is a well-known result and it is a consequence of the fact that the characteristic velocities associated with low-order, largely radial pulsations and low-order, nonradial gravity oscillations are all determined by the gravitational energy of the star.

The Kelvin-Helmholtz or the thermal timescale, $t_{\rm KH}$, is essentially the relaxation time for departures of a star from thermal equilibrium, that is from the timescale necessary to balance the energy generated by thermonuclear reactions in the stellar

interior and the energy lost by radiation (either by photons or by neutrinos) through the stellar surface. If $E_{\rm th}$ is the total internal (thermal) energy of the star and L is its luminosity (net rate of loss of energy through the surface), then $t_{\rm KH} \sim E_{\rm th}/L$. Using the virial theorem (for a stable, self-gravitating, spherical object, the gravitational potential must equal two times the kinetic energy) and assuming that the pressure is supplied by a simple, perfect, nonrelativistic gas, one obtains

$$t_{\rm KH} \sim \frac{3}{4}\frac{GM^2}{LR_\star} \sim 2\times 10^7 \frac{M^2}{LR_\star}\ {\rm yr}, \tag{1.2}$$

where L, M and $R_\star$ are in solar units. The Kelvin-Helmholtz timescale is normally not of immediate interest as far as the periods of pulsating stars are concerned. However, it is relevant in connection with the study of rates of growth or decay of pulsations, that is with the secular changes. Therefore, a more useful dimensionless quantity is the ratio of the dynamic timescale ($\sim$ pulsation period) to the thermal timescale:

$$\frac{t_{\rm ff}}{t_{\rm KH}} \sim \frac{LR_\star^{5/2}}{G^{3/2}M^{5/2}} \sim 10^{-12}\frac{LR_\star^{5/2}}{M^{5/2}}, \tag{1.3}$$

where, again, L, M, and $R_\star$ are in solar units.

Finally, the nuclear timescale, $t_{\rm nuc}$ is only of indirect interest in the study of pulsating stars. However, for the sake of completeness it will be also discussed here. This timescale represents the time required for the properties of a star to change appreciably as a result of the nuclear evolution. For a hydrogen-burning star, and assuming that 10% of the mass is available for thermonuclear reactions, one gets

$$t_{\rm nuc} \sim 10^{10}\frac{M}{L}\ {\rm yr}, \tag{1.4}$$

where, again, M and L are in solar units. A comparison among these timescales usually yields

$$t_{\rm nuc} \gg t_{\rm KH} \gg t_{\rm ff}, \tag{1.5}$$

which is not only true for the sun, but for all the stars which burn hydrogen and helium in a non-explosive manner. However, for more advances stages of stellar evolution some differences may arise.

1.2 Basic equations of stellar pulsations

In the theory of stellar pulsations, there are three basic characteristics of the motions that the associated model may include. That is, the oscillations can be linear or nonlinear, adiabatic or nonadiabatic, and radial or nonradial. Actual pulsations of real stars must certainly involve some nonlinear effects which cannot possibly be explained directly by the linear theory. In fact, the irregular behavior observed in

many variables is definitely not the result of linear combinations of simple sinusoidal waves. Finally, the fact that the observed pulsation amplitudes of pulsating stars of a given type do not show enormous variations from star to star suggests the existence of a limit-cycle behavior typical to nonlinear systems. However the full set of nonlinear equations is so complicated that there are no realistic stellar models for which analytic solutions exist. Accordingly, most recent theoretical studies of stellar pulsations proceed either through pure numerical methods or, conversely, they adopt a set of simplifying assumptions in order to be able to deal with a extraordinarily complex problem.

The advantage of a linear theory is that there are well-known and powerful theorems and methods that can be applied to obtain solutions of the variations and the results appear to be reasonably accurate for a good fraction of the pulsating stars. The linear approximation is the framework in which stability conditions are evaluated and the means by which instability regions in the Hertzsprung-Russell (HR) diagram are determined for large sets of stellar models. In fact, the theory of linear stability is concerned with the question of whether a given solution is stable or not against a small perturbation. This solution could presumably exist in nature more than transiently only if it were stable against every kind of perturbation. If the star is subject to small oscillations about an equilibrium configuration, then it is possible that the star was at one time unstable against such oscillations and that the oscillations would have arisen essentially spontaneously from the instability because of the random fluctuations. Oscillations which arise from an instability against infinitesimal perturbations are often called soft self-excited oscillations. If the oscillation is a pulsation, the system is said to be pulsationally unstable or overstable. Oscillations that grow only after a finite perturbation has been applied to the system are called hard self-excited oscillations.

As a first example of such oscillations, we will discuss small-amplitude motions that are strictly periodic and radially symmetric, that is, linear adiabatic radial pulsations. In this case the time-averaged energy content of the star remains constant, which is the same as saying that the oscillations are adiabatic. It is an approximation based on the assumption that the energy redistribution within the star takes place over time scales which are very long compared to the period of the oscillation ($t_{\rm ff} \ll t_{\rm KH}$). Therefore, all heat exchanges may be ignored, and consequently the system is purely mechanical. Then the problem reduces to studying the behavior of sound waves confined in a box. This approach gives a good dynamic description of many features of actual pulsating stars (it provides reasonably accurate pulsational periods and relatively reliable pulsational amplitudes), but it cannot provide any information about what really causes the star to pulsate (and, hence, we do not obtain any information on the pulsational stability). Moreover, it cannot give us direct information regarding the thermal behavior of the star, and, most important, it cannot provide us with the form of the light curve or the location of the red boundary of the instability strip, since these are clearly nonadiabatic effects. In this case, the mechanical structure can be described using only the mass and momentum conservation

equations together with the adiabatic condition:

$$\frac{\partial M_{\rm r}}{\partial r} = 4\pi r^2 \rho \tag{1.6}$$

$$\ddot{r} = -4\pi r^2 \left(\frac{\partial P}{\partial M_{\rm r}}\right) - \frac{GM_{\rm r}}{r^2} \tag{1.7}$$

$$\Gamma_1 = \left(\frac{\partial P}{\partial M_{\rm r}}\right)_{\rm ad}. \tag{1.8}$$

Linearizing these equations and assuming the standing wave solutions of the form $\zeta(r,t) \equiv \delta r/r = \xi(r)e^{i\sigma t}$, one obtains, after introducing the boundary equations, the so-called Linear Adiabatic Wave Equation, herein after LAWE — see Cox (1980):

$$\mathcal{L}(\xi) \equiv -\frac{1}{\rho r^4}\frac{d}{dr}\left(\Gamma_1 P r^4 \frac{d\xi}{dr}\right) - \frac{1}{r\rho}\left\{\frac{d}{dr}[(3\Gamma_1 - 4)P]\right\}\xi = \sigma^2 \xi, \tag{1.9}$$

where the Sturm-Liouville operator $\mathcal{L}$ is self-adjoint. There are some interesting consequences of this property for stellar pulsations. First, there is an infinite number of eigenvalues, $\sigma_{\rm n}^2$. Second, these eigenvalues are real and can be ordered $\sigma_0^2 < \sigma_1^2 < ...$, with $\sigma_n^2 \to \infty$ for $n \to \infty$. If $\sigma^2 > 0$, then σ is the angular frequency of the associated standing wave. On the contrary if $\sigma^2 < 0$, then σ is imaginary and the perturbations grow/decay exponentially in time.

The LAWE can also be derived in a purely physical way by conceptually displacing a thin mass shell adiabatically from its hydrostatic equilibrium position in a star and then computing the restoring forces acting on the displaced shell. In this way, it comes out that σ^2 is proportional to the force constant of a simple harmonic oscillator. The assumption that σ is constant means that all such shells have the same natural oscillation frequency. In general, a star does not necessarily oscillate in this way. However, a large number of stars (including classical Cepheids, RR Lyrae variables and some W Virginis variables) do appear to be pulsating in this simple way, as if only one mode were present. The simplest (and somehow unrealistic) case is the constant-density or homogeneous model ($\rho(r) = \langle\rho\rangle$). We may consider also homologous motion (ζ constant in space throughout the star as $\partial\zeta/\partial M_{\rm r} = 0$) and that Γ_1 is also constant. Then Eq.(1.9) transforms to

$$\sigma^2 = (3\Gamma_1 - 4)\frac{4\pi G}{3}\langle\rho\rangle. \tag{1.10}$$

Obviously, the importance of the adiabatic index Γ_1 appears very clear. If $\Gamma_1 > 4/3$, σ is real and Eq.(1.10) is just the period-mean density relation. On the contrary, if $\Gamma_1 < 4/3$, then σ is imaginary and the e-folding time for either growth or decay of the motions is

$$\tau = \frac{1}{|\sigma|} = \frac{1}{\sqrt{|3\Gamma_1 - 4|\langle\rho\rangle 4\pi G/3}}. \tag{1.11}$$

which is essentially the free-fall time-scale (corrected for various factors), $t_{\rm ff}$, discussed before.

Before getting into any basic theoretical consideration on stellar hydrodynamics and heat flow, it is worth mentioning the two approaches that are used for describing a general fluid medium: the Eulerian description and the Lagrangian description. The fundamental difference between Eulerian and Lagrangian hydrodynamics lies in the choice of the coordinate system. In the former, all the physical quantities (fluid velocity, total pressure, mass density, temperature) are regarded as functions of position $\mathbf{r}$ and time t, the last ones being the independent variables. The variable $\mathbf{r}$ represents the position of the observation point and can be varied arbitrarily, independently of the time t. In this case, the time derivative taken following the motion of a particular fluid element has the form $D/Dt = \partial/\partial t + \boldsymbol{v} \cdot \boldsymbol{\nabla}$ (i.e., the *Stokes derivative*). In the Lagrangian description, the motion of a particular fluid element is followed and as $\mathbf{r}$ denotes its position, it is no longer an independent variable. Rather, $\mathbf{r}$ is a function of time t and of the position of the element at time $t = 0$, $\boldsymbol{r}_0(r_{1_0}, r_{2_0}, r_{3_0})$. The general advantage of attaching the coordinate system to the fluid (Lagrangian approach) is that the nonlinear terms related to the difference between the observation-point velocity and fluid velocity (advection terms) disappear, making the system much easier to solve. Unfortunately, this is valid only for one dimensional systems, as in two or three dimensions the coordinate quickly deforms following the shear motions of the fluid. Therefore, the Eulerian grid is used for general equations and high-dimensional approaches, paying special attention and effort to solving the difficult advection terms. Fortunately, there exists a method to solve the Lagrangian hydrodynamics that is virtually gridless which is called "Smoothed Particle Hydrodynamics". Its advantages — the simplicity of a Lagrangian approach and the absence of a grid — made it a very successful and powerful computational method (Benz 1991).

In the previous paragraphs it was analyzed the case of linear adiabatic radial oscillations. A very quick view of the more general cases will be given below. The treatment adopted in this section has only descriptive purposes and, therefore, we will not include the heavy calculus — for a detailed analysis, see Cox (1980). Generally, several assumptions are considered independently of the specific model adopted. For instance, turbulence and all forms of viscosity, large-magnetic fields and any composition changes due to nuclear transformations are always neglected in simple models. Let us now consider nonadiabatic terms. The energy equation can be written as:

$$\frac{d\ln P}{dt} = \Gamma_1 \frac{d\ln\rho}{dt} + \rho\frac{\Gamma_3 - 1}{P}\left(\epsilon - \frac{\partial L_{\rm r}}{\partial M_{\rm r}}\right), \tag{1.12}$$

where the second term of the right-hand side represents the nonadiabatic terms and the adiabatic exponent Γ_3 is given by

$$\Gamma_3 - 1 \equiv \left(\frac{d\ln T}{d\ln \rho}\right)_{\rm ad}. \tag{1.13}$$

It is possible to combine Eq.(1.6), (1.7), and (1.12) into a single partial differential equation of third order in time that characterizes the nonlinear nonadiabatic radial oscillations.

$$\begin{aligned}\dddot{r} - \frac{2\dot{r}\ddot{r}}{r} - \frac{4GM_{\rm r}}{r^3}\dot{r} &- 4\pi r^2 \frac{\partial}{\partial M_{\rm r}}\left[4\pi\Gamma_1 P\rho\frac{\partial(r^2\dot{r})}{\partial M_{\rm r}}\right] \\ &= -4\pi r^2\frac{\partial}{\partial M_{\rm r}}\left[\rho(\Gamma_3-1)\left(\epsilon - \frac{\partial L_{\rm r}}{\partial M_{\rm r}}\right)\right]. \end{aligned}\tag{1.14}$$

Since the system is now no longer conservative, there can exist solutions with complex frequencies, that is solutions characterized by secularly increasing (driving or unstable) or decreasing (damping or stable) pulsation amplitudes. It is therefore possible to investigate the important question of pulsational stability, or in other words, the causes of pulsations in stars, as an intrinsically variable star is one in which the nonadiabatic effects drive the star to pulsational instability.

1.3 Mechanisms of driving

Adiabatic radial pulsations in stars are relatively well understood. However, the intrinsic variability of some stars implies that something inside the star causes the pulsation, while the adiabatic pulsations have no beginning, end or apparent cause. In order for a star to present sustained oscillations, the gases comprising the layers participating to the pulsation must do net positive PdV work on its surroundings during one entire period. In the case of a negative net work, they contribute to the damping of the oscillations.

As the work performed during one cycle is the integral of the absorbed heat, a more precise form of the integral work W can be obtained by considering it as an integral over the shells of mass $dM_{\rm r}$ characterized by the heat exchange dQ:

$$\begin{aligned} W &= \int_M \oint \frac{\delta T}{T} dQ\; dM_{\rm r} \\ &= \int_M \oint \frac{\delta T}{T}\left[\delta\epsilon - \delta\left(\frac{1}{\rho}\nabla\cdot(\boldsymbol{F}_{\rm rad}+\boldsymbol{F}_{\rm conv})\right)_{\rm r}\right] dt\; dM_{\rm r}, \end{aligned}\tag{1.15}$$

with $W > 0$ being the driving condition (initial perturbations will increase) and $W < 0$, the damping condition (stability). The effect of nuclear reactions ($\delta\epsilon > 0$, with ϵ being the thermonuclear energy production per unit mass) is to push the stars toward instability. This is called the *ϵ-mechanism*: ϵ increases and adds heat to a

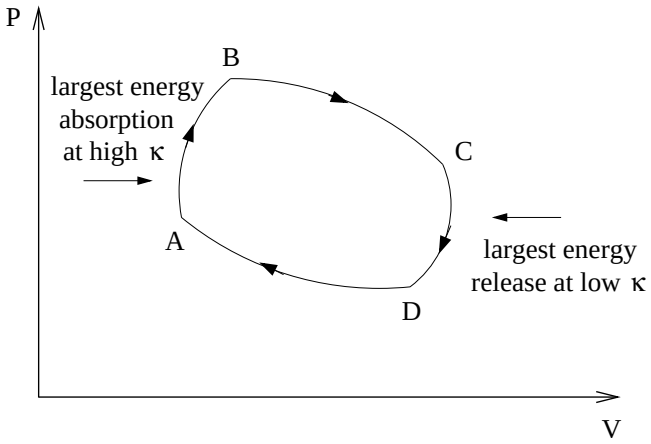

Figure 1.1: The κ-mechanism in the pressure-volume diagram. DA: adiabatic compression, with maximum contraction velocity attained in D; AB: energy increase by increasing κ leading to increasing pressure; BC: adiabatic expansion; CD: energy release by decreasing κ leading to maximum luminosity in D. Adapted from de Loore & Doom (1992).

compressing element which is exactly the driving criterion expressed above. However, no intrinsically variable star has been shown to be unstable due to this effect, but this mechanism seems to be the cause of mass limitation of the main sequence at higher luminosities.

The true mechanism for intrinsic variable stars was first proposed in Eddington (1917) and further developed in Eddington (1919) where it was suggested the existence of a *valve mechanism* due to which these stars behave as thermodynamic heat engines: heat is absorbed ($dQ > 0$) when the temperature is increasing ($\delta T > 0$) — see Figure 1.1. In order for this mechanism to be possible, the opacity must increase as the mass shell is compressed. From the general formula of opacity (Kramers law)

$$\kappa \propto \rho^n T^{-s} \,, \tag{1.16}$$

with $n = 1$ and $s = 3.5$, it results that the opacity usually decreases upon compression as, even if both temperature and density increase during compression, κ is more dependent on the temperature due to its power of 3.5. However, it takes special conditions for the driving to overcome the damping effect of most stellar layers, conditions that were discovered significantly later than the first works of Eddington (Zhevakin, 1963) and concern the partial ionization regions in the star. In these zones, ionized particles are created during compression and this leads to heat absorption and a smaller increase in temperature than in other regions. This translates into the density increasing more than the temperature, and thus the opacity increases. This in turn traps the heat and starts the expansion of the star. Now during the expansion, the temperature does not drop by as much as would be expected because the ions recombine with the electrons producing energy as they do so. The

density also decreases which in turn lowers the opacity, allowing the star to contract and start the cycle again. This mechanism is referred to as the *κ-mechanism*.

There are two main ionization regions: the first one is the hydrogen partial ionization zone, which is a broad region where both HI $\rightarrow$ HII and HeI $\rightarrow$ HeII occur, being its typical temperature of 1 to 1.5×10^4 K; whereas the second one is a deeper zone which involves the HeII $\rightarrow$ HeIII ionization and, hence, it is known as the HeII partial ionization zone, being its temperature of about 4×10^4 K. The ability of these zones to produce pulsational instability in stars arises essentially from the fact that the ionization of an abundant element can result in modulations of the flux variation — the right-hand side of Eq.(1.15). Detailed calculations show that in most stellar pulsators within the instability strip (classical Cepheids, RR Lyrae and W Vir stars) it is indeed the combination of HI and HeII ionization zones which is responsible for driving the oscillations, while the same role is played by the HI ionization zone for Long Period Variables (hereafter, LPVs) and by the C and O ionization regions for the variable planetary nebulae nuclei (PG 1159 objects). Moreover, the efficiency of the excitation mechanisms extends to some pre-white dwarfs — DOV or GW Vir variables, see Cox (2003) — driven by the C/O partial ionization, and in different families of white dwarfs: the DB driven by HeII ionization and the DA (the ZZ Ceti objects) corresponding to the extension of the instability strip below the main sequence, to lower luminosities (Figure 1.2).

If s in Eq.(1.16) is large and negative (as may be the case in the HI zones), there may be driving, even if Γ_3 has a value close to the normal one of 5/3. In particular, at the temperature ($\approx 1.5 \times 10^5$ K) at which the photon energy in the maximum-energy peak in the radiation field is close to the ionization potential (54.4 eV) of HeII, there is an increase in the opacity because s becomes less positive than usual which, again, produces driving. This is the so-called *bump mechanism* (Stellingwerf, 1979). It is expected to be more efficient for stars departing from main sequence than for giants. Another enhancement in the opacity corresponds to temperatures between $1 - 3 \times 10^5$ and is due to intra-M-shell transition in Fe. It is generally called *Z-bump mechanism* and appears to produce the variability of the β-Cephei stars and to enhance the pulsational instability in all the other variable stars (Figure 1.2).

The most important effect of such ionization zones is that $\Gamma_3 - 1$ becomes rather small in such regions. Most of the work on adiabatic compression goes into ionizing the corresponding chemical species rather than into thermal energy of the mass shell (and, hence, $\delta T/T$ is smaller). Since the luminosity scales as $L_{\rm r} \propto T^4$, for a given opacity κ, the flow of radiation is locally diminished upon compression and the radiation is absorbed by the matter in the region of decreasing $\Gamma_3 - 1$ at the instant of the largest compression. This absorption causes the temperature, and therefore the pressure, to be slightly larger during the ensuing expansion. This mechanism is referred to as the *γ-mechanism*. In Figure 1.2 we represent the regions in the Hertzsprung-Russell diagram which provide the distinct classes of pulsating stars as well as their main excitation mechanism. Also shown are the main sequence (dashed line), the white dwarf colling curve (dot-dot-dashed line) and the evolutionary tracks (solid

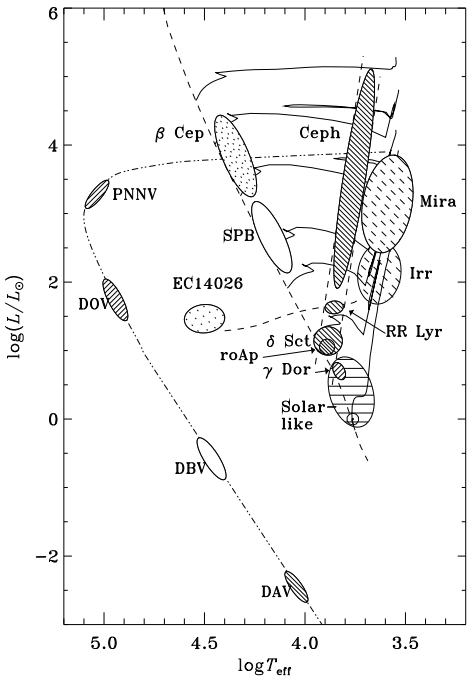

Figure 1.2: Hertzsprung-Russell diagram illustrating several classes of pulsating stars. Pulsation is due to HI ionization zone *(left-inclined dashed)*, HI and HeII ionization zones *(left-inclined solid)*, HeII ionization zone *(white regions)*, the Z-bump mechanism *(dotted regions)* and to C/O ionization regions *(right-inclined solid)*. Adapted from Christensen-Dalsgaard (2003).

lines) for 1, 2, 3, 4, 7, 12 and 20 $M_\odot$.

The contribution of all these mechanisms (the κ-, γ- and the bump-mechanisms) to the sign of the work integral associated to a radiative envelope with no nuclear burning is best reflected in Eq.(35) of Gautschy & Saio (1995)

$$\mathrm{sign}(W) = \mathrm{sign}\left[\frac{d}{dr}\left(-s + \frac{n}{\Gamma_3 - 1}\right)\right]. \tag{1.17}$$

The location of the ionization zones within the star determines its pulsational properties. Indeed, the excitation mechanisms win over damping only if the zones of ionization, which provide the excitation, contain a sizable fraction of the mass of the star. In order to fulfill this requirement these zones have to be located at suitable depths. Since ionization is mainly a function of the temperature, it results that it is essentially the surface temperature which determines whether the star is vibrationally stable or unstable via the κ-mechanism. At effective temperatures slightly below and above the instability strip, the He II ionization zones are located either too deep ($T_{\rm eff}$ low) or too high ($T_{\rm eff}$ high) for them to be effective (Carroll & Ostlie, 1996). And for these cases, the H ionization zone is located either not deep enough or too high for it

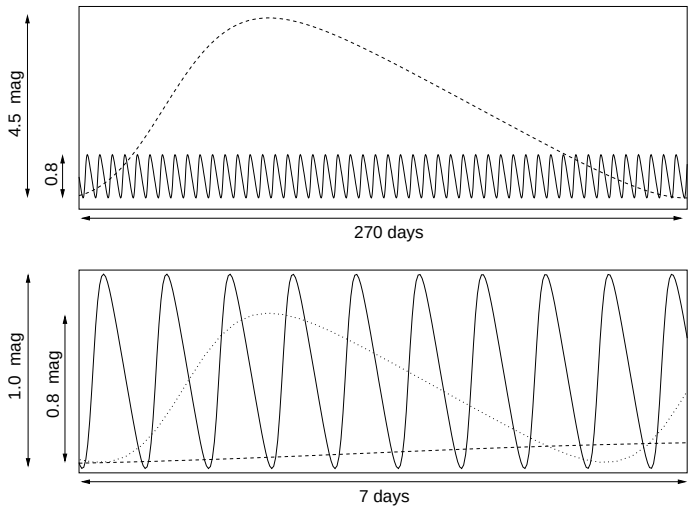

Figure 1.3: Schematic view of the variability of the RR Lyrae (solid line), Classical Cepheids (dotted line) and Long-Period Variables (dashed line). Adapted from Malatesta (2002).

to work, and it is necessary a lower $T_{\rm eff}$ for it to become a driving region — this is the case of the LPVs. However, when considering models with still lower effective temperatures, one has to keep in mind that Eq.(1.15) holds only in radiative regions, and therefore a proper treatment of the pulsation-convection interaction is imperative. It is expected that the κ/γ interaction be weakened or even disabled if convection can transport away some of the energy trapped in the ionization regions. However, there exist results suggesting the existence of convection-induced oscillations (Wood 2000) which might shed some light on the newly-discovered and still-unexplained period-luminosity law for lone-period variables (Wood et al. 1999).

As we have seen, the instability strip contains the pulsating stars which are vibrationally unstable via the κ-mechanism. The star models of masses between 5 and 10 $M_{\odot}$ loop horizontally back and forth during the phase of core helium burning, thereby passing through the instability strip at least twice. Depending on their mass, the passages occur at quite different luminosities. In fact, and as a general result, it can be said that the larger the mass, the higher the luminosity and the longer the period (see the Cepheid instability strip in Figure 1.2). In the present thesis we shall be concerned mainly about long-period variables and in some particular cases, the stars of the Cepheid instability strip. For comparative and completness reasons we present in Figure 1.3 a schematic view of the pulsational characteristics of these type of variables.

However, the position on the HR diagram does not automatically render the pulsational properties of the star. In fact, it depends notably on the chemical composition. For instance, assume that two stars are situated at the same point in the HR

diagram, a Population I star and a Population II star. Being at the same point in the HR diagram, they have the same radii, temperature and luminosity, but the larger metal content of Population II stars implies higher opacities, therefore less transparency and lower mean density. The period-density relation (Eq. 1.10) yields a longer period than in the case of a Population I star. Therefore, pulsating Population I stars have always higher luminosities than pulsating Population II stars of the same period (de Loore & Doom, 1992).

Chapter 2

One-zone models for stellar pulsations

Nonadiabatic stellar pulsations are definitely a complicated phenomenon even for very small amplitudes and for purely radial oscillations, where the linear theory is applicable. For larger amplitudes where nonlinear effects are more important, the situation is almost hopeless. Most of the simple models of stellar pulsations are based on a one-zone type of model which may be visualized as a single, relatively thin, spherical mass-shell concentric with the stellar center. These models have helped considerably in clarifying some of the complicated physics involved in stellar pulsations and the role played by different physical mechanisms. In this chapter we describe the most relevant and successful of such simple models. This short review is motivated by the important role played by these models in the formulation of our approach to the study of stellar oscillations.

A one-zone model — see Schatzman et al. (1993) — is characterized by a shell of mass $\Delta M_{\rm r}$ at radius $r(t)$ on top of a region called the core of mass $M_{\rm c}$ and radius $r_{\rm c}$ which provides a luminosity $L_{\rm c}$. Synthetically, the behavior of the zone is governed by the equations

$$\frac{d^2r}{dt^2} = g(r,s) \tag{2.1}$$

$$\frac{ds}{dt} = \xi h(r,s), \tag{2.2}$$

where s is the specific entropy, ξ is the ratio of the dynamic and thermal timescales, while the total acceleration, $g(r,s)$ and the entropy production rate, $h(r,s)$ are given by

$$g(r,s) = -\frac{GM_{\rm r}}{r^2} + 4\pi r^2 \frac{P(\rho,s)}{\Delta M_{\rm r}} \tag{2.3}$$

$$h(r,s) = \frac{L_{\rm c} - L}{\Delta M_{\rm r} T(\rho,s)}. \tag{2.4}$$

The functions $P(\rho, s)$, $T(\rho, s)$ are given by the equation of state taking into account the ionization change during the motion, and ρ is given by mass conservation for the one-zone model, $4\pi\rho(r^3 - r_c^3) = 3\Delta M_r$. The luminosity L in the shell is obtained using the radiative energy transport law in the diffusion approximation

$$L_r = -\frac{64\pi^2 acr^4 T^3}{3\kappa}\frac{dT}{dM_r}, \tag{2.5}$$

with a being the radiation density constant and c, the speed of light. A star in dynamically stable hydrostatic equilibrium, but not in thermal equilibrium will evolve away from this equilibrium on a thermal timescale. When this happens, the right-hand side of the thermal-balance equation (2.2) does not vanish:

$$\frac{ds}{dt} = \frac{1}{T}\left(q - \frac{dL_r}{dM_r}\right), \tag{2.6}$$

where q represents local energy sources and (dL_r/dM_r) the divergence of the flux. As a result the entropy s depends on time. If there is sufficient energy available, then the thermal instability and the dynamic instability have opposite effects. A large variety of oscillatory motions are then possible, including relaxation oscillations. In particular, if the dynamic and thermal timescales are comparable, irregular variations can occur.

2.1 The one-zone model of Baker

The one-zone model of Baker (1966) was primarily designed for dealing with very small, radial oscillations, that is for elucidating some physical problems which can be described with linear physics. The model is represented by a single spherical shell of mass ΔM_r considered as the envelope in which all the physical variables (except the variations of luminosity) are assumed to be constant in space, and that $\epsilon = 0$. For this case, in the linearized mass, energy and momentum conservation equations all the spatial derivatives are dropped except $\partial(\delta L_r/L_r)/\partial M_r$. A further approximation is done by assuming that

$$\frac{\partial}{\partial M_r}\left(\frac{\delta L_r}{L_r}\right) = \frac{2}{\Delta M_r}\left(\frac{\delta L_r}{L_r}\right), \tag{2.7}$$

where the factor 2 appears from considering that the small variations in the luminosity of the shell are the mean average of luminosity fluctuations of the upper and lower boundary of the shell, with the latter being taken as zero. Additionally, the transfer of energy is considered to be only radiative and the opacity is given by Eq.(1.16). Assuming also a time dependence for all pulsation variables of the form $e^{\lambda t}$ and combining the above-mentioned equations and the linearized equation of state

$$\frac{\delta P}{P} = \chi_\rho\frac{\delta\rho}{\rho} + \chi_T\frac{\delta T}{T}, \tag{2.8}$$

where χ denotes the logarithmic partial derivate of the pressure with respect to the relevant physical variable. The result is the following cubic equation for the eigenvalues λ:

$$\lambda^3 + K\sigma_0 A\lambda^2 + B\sigma_0^2\lambda + K\sigma_0^3 D = 0\,, \tag{2.9}$$

where

$$A \equiv (\Gamma_3 - 1)(s+4)/\chi_\rho \tag{2.10}$$
$$B \equiv 3\Gamma_1 - 4 \tag{2.11}$$
$$D \equiv (\Gamma_3 - 1)[3n\chi_T - s(4 - 3\chi_\rho) + 4(\chi_T + 3\chi_\rho - 4)]/\chi_\rho \tag{2.12}$$
$$K \equiv \frac{\chi_\rho}{\Gamma_3 - 1}\frac{2L}{\Delta M_{\rm r} c_{\rm V} T}\frac{1}{\sigma_0} \tag{2.13}$$
$$\sigma_0^2 \equiv GM/R_\star^3, \tag{2.14}$$

while all the other symbols have their usual meaning. For $K = 0$, which corresponds to an adiabatic motion, the only non-vanishing roots of Eq.(2.9) are

$$\begin{aligned}\lambda_0 &= \pm i(3\Gamma_1 - 4)^{1/2}\sigma_0 \\ &= \pm i[(3\Gamma_1 - 4)\frac{4\pi G}{3}\overline{\rho}]^{1/2},\end{aligned} \tag{2.15}$$

where

$$\overline{\rho} \equiv \frac{M_{\rm r}}{\frac{4}{3}\pi r^3} \tag{2.16}$$

is the average density of the region interior to radius r. If $\Gamma_1 > 4/3$, these roots are purely imaginary, corresponding to pulsations of constant amplitude. If $\Gamma_1 < 4/3$, both roots are purely real, corresponding to exponential increase or decrease in perturbation, both cases being denominated dynamic instability. Thus, the condition of dynamic stability is $B > 0$.

For the case of $K \neq 0$, two additional stability conditions are necessary so that the one-zone model shall be stable with respect to all radial motions. The condition for secular stability is $D > 0$. To illustrate this condition, one can start by considering that there exists the root of Eq.(2.9) given by

$$\lambda_s \approx -\frac{K\sigma_0 D}{B} = -\frac{K\sigma_0 D}{3\Gamma_1 - 4}, \tag{2.17}$$

which is purely real (aperiodic motion) for $D > 0$ (and, of course, $\Gamma_1 > 4/3$). This is the smallest possible root. The time scale of this motion, $1/\lambda_s$, is of the order of $(L/c_{\rm V} T\Delta M_{\rm r})^{-1}$, which is clearly the thermal time scale of the zone. For the particular case of $\chi_\rho = \chi_T = 1$ (a simple perfect gas), the condition of secular stability

becomes: $3n - s > 0$, which means that $\delta L_{\rm r}/L_{\rm r}$ must decrease upon compression (stable configuration). The condition for pulsational stability is

$$AB - D > 0, \tag{2.18}$$

which comes from considering the roots of Eq.(2.9) as first-order expansions in terms of K, that is $\lambda = \lambda_0 + \lambda_1 K$:

$$\lambda_{2,3} \approx \pm iB^{1/2}\sigma_0 - \frac{\sigma_0(AB - D)}{2B}\, K + ... \tag{2.19}$$

A more physical version of Eq.(2.18) is

$$4(\Gamma_3 - 1) + [s(\Gamma_3 - 1) - n] - \frac{4}{3} > 0. \tag{2.20}$$

The first term, $4(\Gamma_3 - 1)$, is always positive, and therefore always tends to stabilize. This term represents cooling upon compression as a result of enhanced radiation flow at this moment ($L_{\rm r} \propto T^4$ and $T \propto \rho^{\Gamma_3 - 1}$ in the adiabatic approximation). In an ionization zone of a dominant element, $\Gamma_3 - 1 \rightarrow 0$ and, thus, the damping effects are diminished. That is, the ionization prevents the temperature from rising very much upon compression and hence inhibits the loss of radiation at this moment. It is practically the γ-mechanism. The second term, $s(\Gamma_3 - 1) - n$, gives the effect of the opacity variations and can be of either sign. For the normal values $n \approx 1,\ s \approx 3,\ \Gamma_3 - 1 \approx 2/3$, this term is positive and therefore contributes to the damping. For ionization zones, this term can be negative as $\Gamma_3 - 1 \rightarrow 0$ and therefore contributes to the driving (κ-mechanism). If s is large and negative, this term would represent trapping of radiation during compression, and hence driving, even if Γ_3 had its normal value of about 5/3. It is the bump mechanism. The third term, $-4/3$, which arises from the assumed spherical symmetry, being negative, always tends to destabilize. It merely reflects the dependence of the local luminosity on the area of the spherical surface of the mass region of interest ($L_{\rm r} \propto r^4$). The area of this surface becomes smaller upon compression, thus producing trapping of radiation, and hence a destabilizing tendency. This effect of curvature is usually referred to as the radius effect or "throttling effect" (Baker 1966).

2.2 The model of Moore & Spiegel

The model of Moore & Spiegel (1966) was constructed for studying overstability in a convectively unstable zone. The equation of motion of an oscillating mass immersed in a horizontally stratified fluid was obtained by Moore & Spiegel in the form

$$\frac{d^3z}{dt^3} + q\frac{d^2z}{dt^2} - \left(g\alpha\beta + \frac{dr}{dz}\right)\frac{dz}{dt} - qr(z) = 0, \tag{2.21}$$

where z is the displacement of the mass element, g is the gravitational acceleration, α is the thermal expansion coefficient from the Boussinesq approximation, while the temperature gradient, β and the restoring force, $r(z)$ are defined for small oscillations as

$$\beta(z) = -\frac{T_0(z)}{dz} = \beta_0 + 0(z) \ , \ \ r(z) = -\lambda^2 z + O(z^2) \ , \tag{2.22}$$

with T_0 being the ambient temperature and λ and β_0 real constants. Additionally, the characteristic time for radiative damping, q^{-1}, results from the evolution of the temperature as $dT(t)/dt = -q[T(t) - T_0(z)]$. In the first approximation, Eq.(2.21) becomes

$$\frac{d^3z}{dt^3} + q\frac{d^2z}{dt^2} - [(g\alpha\beta_0 - \lambda^2) - g\alpha\beta_0 z^2]\frac{dz}{dt} + q\lambda^2 z = 0. \tag{2.23}$$

In the case of adiabatic motion, Eq.(2.23) leads to a cubic equation for the eigenvalues of the type

$$(\Lambda - 1)z + z^3/3 = b, \tag{2.24}$$

where $\Lambda \equiv \lambda^2/g\alpha\beta_0$ and b a constant of integration. The analysis of the cubic equation shows that for $\Lambda > 1$, it has one root, whatever b is, while for $\Lambda < 1$, it has one real root for $|b| > b_{\rm c}$, with $3b_{\rm c} \equiv 2(1-\Lambda)^{3/2}$, and three real roots for $|b| < b_{\rm c}$. More precisely, in the phase plane $(z, \dot{z})$, the case $\Lambda < 1$ will show two stable fixed points of elliptic type and one unstable fixed point between them of hyperbolic type (see Appendix A). For $\Lambda > 1$, the phase plane will show one elliptic fixed point.

When dissipation is introduced ($q \neq 0$), a new property of the trajectories in the phase plane appears: period doubling. For $q = 0$, the system has a periodic orbit of period Π; for $q \neq 0$ and small, the orbit is still periodic, but closes only after a period 2Π — this is the first bifurcation. As q increases, the orbit is still periodic, but now with periods 2Π and 4Π, with the orbit closing after 4Π. As the parameter q is increased more bifurcations appear, and the distance between successive bifurcations $(q_{n+1} - q_n)$ decreases. There is a critical value, q_∞, above which the orbits are no longer regular at all and the dynamic system becomes chaotic — see also Schatzman et al. (1993). The mathematical details of this model with emphasis on the aperiodic behavior were explored thoroughly in Baker et al. (1971).

2.3 The model of Rudd & Rosenberg

The one-zone model of Rudd & Rosenberg (1970) tried to clarify some of the mathematics underlying fully nonlinear stellar pulsations and the occurrence of limit cycle-like phenomena of the kind observed in real pulsating stars. More specifically, they wanted to devise a model which would exhibit overstability at small amplitudes and a stable limit cycle at large amplitudes. The model is obtained as follows. If $M_{\rm r}$ is

the mass of the rigid core, $\Delta M_{\rm r} \ll M_{\rm r}$ is the mass of the gas in the shell, and r the instantaneous radius of the shell, then the equation of motion of the shell is taken to be

$$\frac{d^2r}{dt^2} = -4\pi r^2 \frac{P}{\Delta M_{\rm r}} - \frac{GM_{\rm r}}{r^2}, \tag{2.25}$$

being P, as usual, the pressure of the gas. The equilibrium radius, r_0, of the shell results from setting the acceleration equal to zero in Eq.(2.25). The energy equation is introduced as the integral form of Eq.(1.12), that is

$$\frac{P}{P_0} = \left(\frac{\rho}{\rho_0}\right)^{\Gamma_1} K(1 - \frac{r}{r_0}), \tag{2.26}$$

where K is a function of $(1 - r/r_0)$ which incorporates the nonadiabatic effects of the pulsation mechanism and whose nature is determined from astronomical data.

The relation radius-density for this model follows the one from Usher & Whitney (1968) written in the form

$$\frac{\rho}{\rho_0} = \left(\frac{r}{r_0}\right)^{-m}, \tag{2.27}$$

where

$$m \equiv \frac{1}{\ln(r/r_0)} \ln\left[\frac{(r/r_0)^3 n_0^3 - 1}{n_0^3 - 1}\right], \tag{2.28}$$

being $n_0 = r_0/r_{\rm c} \geq 1$, and $r_{\rm c}$ the radius of the core. If $r \approx r_0$, then m becomes a constant depending only on n_0,

$$m = \frac{3n_0^3}{n_0^3 - 1}. \tag{2.29}$$

Should the core be of zero radius ($n_0 = \infty$), it would give the homogeneous model, that is $m = 3$. One can see that if n_0 is finite then $m > 3$. The authors argue that a value of $m \approx 12$ corresponding to $n_0 \approx 1.2$ might be appropriate for real pulsating stars for which only the outermost layers are effectively pulsating. With these assumptions, the final equation of motion of the model is

$$\ddot{x} = \frac{GM}{r_0^3}\left[\frac{K}{x^q} - \frac{1}{x^2}\right], \tag{2.30}$$

where $x \equiv r/r_0$, $q \equiv m\Gamma_1 - 2$. The dynamic stability condition (i.e., the existence of oscillatory solutions) now becomes $m\Gamma_1 - 4 > 0$ instead of the previously obtained $\Gamma_1 > 4/3$. The main novelty of this model consists in regarding the expansion and contraction phases as qualitatively different: these two phases appear to occur about two different equilibrium radii, the one for the expansion being larger than that for contraction. The difference consists in the functional forms of K:

$$K_{\rm e} = E_0 + E_2(1-x)^2 \tag{2.31}$$
$$K_{\rm c} = C_0 + C_2(1-x)^2, \tag{2.32}$$

where the subscripts "e" and "c" refer, respectively, to the expansion and contraction phases. The quadratic terms are chosen in accordance with the requirement that K should never be negative. The same considerations also require that $E_0,\ C_0,\ E_2,$ and C_2 should all be positive numbers. The transitions between Eq.(2.31) and Eq.(2.32) are assumed to occur discontinuously at the end of successive phases of expansion and contraction. However, x and $\dot{x}$ are assumed to be continuous throughout the motion, while $\ddot{x}$ changes discontinuously at the end of each phase of expansion and of contraction. Another necessary condition is $E_0 > 1 > C_0$. In the limit of small amplitudes ($x \approx 1$), the condition $E_0 > C_0$ leads to a built-up of the amplitude (self-excitation of the pulsations). Also, treating K as a constant during half-cycles is equivalent to assume that the motion is adiabatic during each half-cycle, but nonadiabatic for an infinitesimal time at each turn-around point. In other words, the model is piecewise conservative, but globally nonconservative.

The limitation of the amplitude and the occurrence of a limit cycle are produced by the quadratic terms, while the existence of a stable limit cycle is given by the necessary and sufficient condition $C_2 > E_2$. Physically, it means that nonadiabatic effects must produce a relative strengthening of the outward restoring forces when the gas is moving inward toward minimum radius, and a relative weakening of the inward restoring force when the gas is expanding away from minimum radius, if a limit cycle is about to exist.

2.4 The model of Castor

The main purpose of this model was to investigate the problem of the amplitude limitation for soft self-excited oscillations. In Castor (1971) — see also Cox (1980) — it is first noted that for adiabatic motion, pulsations of every amplitude are possible. He thus reasoned that the main physical cause of amplitude limitation is likely to be found in nonlinearities in the nonadiabatic part of the motion. This conclusion is consistent also with the amplitude-limiting mechanism of the Rudd-Rosenberg model. He noticed that the general, nonlinear, nonadiabatic third-order partial differential equation Eq.(1.14) has all explicit nonadiabatic effects contained in the right hand side. Therefore, he linearized only the left hand side, while the right hand side was expanded into a linear term plus one higher order term. Finally, in this model, Eq.(2.27) is written as

$$\frac{\dot{\rho}}{\rho} = -m_{\rm r}\frac{\dot{r}}{r}, \tag{2.33}$$

where

$$m_{\rm r} \equiv \frac{3n_0^3}{n_0^3-1}\left(\frac{r}{r_0}\right)^3\left(\frac{\rho}{\rho_0}\right), \tag{2.34}$$

using the same notation of Eq.(2.27) and Eq.(2.28). The final nonlinear equation has the form

$$\begin{aligned}\dddot{r} - \frac{\dot{r}\ddot{r}}{r}(m_{\rm r}\Gamma_1 - 2) \;&+\; (m_{\rm r}\Gamma_1 - r)\frac{GM}{r^3}\dot{r} = \\ &= 4\pi r^2\frac{\rho(\Gamma_3-1)}{\Delta M_{\rm r}}\left(\epsilon - \frac{\partial L_{\rm r}}{\partial M_{\rm r}}\right).\end{aligned} \tag{2.35}$$

In linearizing the left hand side one assumes that the unperturbed model is in hydrostatic equilibrium ($\ddot{r_0} = 0$) and that Γ_1 is constant. Also, a characteristic angular frequency can be defined as

$$\omega_0 \equiv \left[(m_0\Gamma_1 - 4)\frac{GM}{r_0^3}\right]^{1/2}, \tag{2.36}$$

where m_0 is the value of $m_{\rm r}$ in the unperturbed model and $\Gamma_1 \geq 4/m_0$, so that ω_0 is purely real. Now, expanding the right side of Eq.(1.46) into a linear term $\zeta \equiv \delta r/r$ and a cubic term in ζ and defining a new time scale as $\tau \equiv \omega_0 t$, one gets the final form of Eq.(2.35) as

$$\frac{d^3\zeta}{d\tau^3} + \frac{d\zeta}{d\tau} + \epsilon(\zeta - Q\zeta^3) = 0, \tag{2.37}$$

where ϵ and Q are two parameters. For certain conditions, Castor obtained four limit cycles, but only one of these was found to be stable.

2.5 The model of Stellingwerf

The one-zone model from Stellingwerf (1972) is an extension of the Rudd & Rosenberg model and definitely inspired in that of Usher & Whitney (1968). From the Rudd-Rosenberg model, Stellingwerf takes the momentum equation, that is Eq. (2.25), and the geometry equations — namely Eq.(2.27) and Eq.(2.28). Using the equilibrium condition $d^2r_0/dt^2 = 0$ and the notation $X \equiv r/r_0$, it can be easily shown that the equation of motion becomes

$$\frac{d^2X}{dt^2} = \frac{GM}{r_0^3}\left[\left(\frac{P}{P_0}\right)X^2 - X^{-2}\right]. \tag{2.38}$$

He furthermore introduced the notation $\tau \equiv t/\Pi$ — being Π the period of oscillation — and the quantity ξ, defined as

$$\xi = \frac{GM}{r_0^3}\Pi^2. \tag{2.39}$$

The nonadiabatic effects are contained in the function H defined by

$$\frac{P}{P_0} = \left(\frac{\rho}{\rho_0}\right)^{\Gamma_1} H. \tag{2.40}$$

With these definitions, the final equation of motion turns out to be

$$\frac{d^2X}{d\tau^2} = \xi(HX^{-(m\Gamma_1-2)} - X^{-2}), \tag{2.41}$$

where m is defined in Eq.(2.28). In order to obtain the variation of the function H, the energy equation is used in the form

$$\frac{\partial P}{\partial t} = \frac{\Gamma_1 P}{\rho}\frac{\partial \rho}{\partial t} - \rho(\Gamma_3 - 1)\frac{\partial L_{\rm r}}{\partial M_{\rm r}}, \tag{2.42}$$

where the thermonuclear production rate has been neglected ($\epsilon = 0$). In order to allow for a possible variation of the luminosity interior to the inner boundary of the pulsating region, he assumes the form $\partial L_{\rm r}/\partial M_{\rm r} \approx (L - L_{\rm i})/\Delta M_{\rm r}$, where $L_{\rm i}$ is the luminosity of the rigid core. The luminosity in the case of radiative transport of energy is given by

$$L_{\rm r} = -\frac{64\pi^2 acr^4T^3}{3\kappa}\frac{dT}{dM_r}, \tag{2.43}$$

with a being the radiation density constant and c, the speed of light. For the one-zone model, this formula translates into

$$\frac{L}{L_0} = X^4\left(\frac{T}{T_0}\right)^4\left(\frac{\kappa}{\kappa_0}\right)^{-1}, \tag{2.44}$$

with L_0 being the equilibrium luminosity of the model and κ, the opacity, while Eq.(2.42) becomes

$$\frac{dH}{d\tau} = -\zeta X^{m(\Gamma_1-1)}[X^bH^{s+4} - L_{\rm i}/L_0], \tag{2.45}$$

where s is defined in Kramers law of opacity (Eq.1.16) and

$$b = 4 + m[n - (s+4)(\Gamma_1 - 1)] \tag{2.46}$$

$$\zeta = \Pi\frac{\rho_0 L_0}{P_0\Delta M_{\rm r}}(\Gamma_3 - 1) = \frac{L_0\Pi}{E_{\rm s}}. \tag{2.47}$$

In other words, the nonadiabaticity parameter, ζ, is the ratio of the total radiated energy during one period to the total internal energy of the shell, $E_{\rm s}$. As in

Cox (1980), ζ is considered to be almost unity in the instability strip, while having high values in the ionization regions of hot stars and low values for cool stars. It is worth noticing that the values and forms of ζ constitute a very controversial matter, implying distinct analytic forms and values (Ostlie & Cox 1986; Saitou et al. 1989). In connection with ζ, it is also of interest the elegant approach from the old but still actual work of Usher & Whitney (1968) where their solution led to a significant alteration of the oscillation frequency associated with the variations of entropy, with the frequency change being of second order in ζ.

In the model of Stellingwerf, Eqs.(2.41, 2.45) constitute the final set of relations for the unknowns X and H. Taking $n = 1$, $s = 3$, $L_{\rm i}/L_0 = 1$ and n_0 such that the shell thickness comprises $10-15\%$ of the stellar radius, the three basic parameters of this model remain Q, ξ and Γ_1. The model yields an approximate value of 90° phase lag in the emergent luminosity variation which is thought to be caused by the combination of damping in the interior and driving in the shell. This phase lag is observed in the majority of Cepheids. Stellingwerf also shows that the linear one-zone formulation agrees quite well with the nonlinear results as far as the phase shift and the luminosity amplitude are concerned. However, in contrast to the Rudd-Rosenberg model, the Stellingwerf model does not possess a built-in amplitude-limiting mechanism.

2.6 Other simple models

Buchler & Regev (1982) developed a simple one-zone model of interest for the oscillations in stars with extended convective partial ionization regions, which is very similar to the Moore & Spiegel (1966) oscillator. Later, Tanaka & Takeuti (1988) have shown that the Rössler dynamic system (Strogatz 1994) can be considered a fare model of stellar oscillations. Kovács & Buchler (1988) later found that chaotic pulsations in the numerical hydrodynamic modeling of W Vir stars seem to have the topology of the Rössler attractor. Saitou et al. (1989) argued in a one-zone treatment that the saturation by large-amplitude dissipation can explain the semi-regular variability of yellow giants. In a more mathematical approach, Unno & Xiong (1993) formulated a theoretical one-zone modeling of the irregular variability in red supergiants considering the nonlinear coupling of finite amplitude pulsation with convection. Another approach to convection treatment is the extension of the abovementioned Stellingwerf model to include the treatment of convection in Stellingwerf (1986). A previous step toward the study of the pulsation-convection interaction in simple models was done by Pesnell (1985). While there is strong evidence that, to some degree, pure radiative models are inconsistent with the observations (Buchler 1998) and that a treatment of pulsation-convection interaction in red giants is indispensable, no common agreement exists yet neither on its form nor on its influence on the pulsation.

Chapter 3

One-zone model for Super-AGB stars

Long term photometry of several LPVs has revealed not only regular light curves, but also irregularities superimposed onto the regular variations, which lead to a high degree of unpredictability. Due to the lack of appropriate tools for analyzing these irregular fluctuations of the luminosity or the stellar radius, the scientific community did not pay much attention to this category of variable stars. The development of new nonlinear time-series analysis tools during the last decade has changed this perspective. In particular, it has been found that these tools have rich applications in a broad range of astrophysical situations, which include wavelet analysis of gamma-ray bursts (Norris et al. 1994), of variable white dwarfs (Goupil et al. 1991), of gravitationally lensed quasars (Hjorth et al. 1992) or X-rays within galaxy clusters (Slezak et al. 1994). To be more specific, in the field of stellar variability, Serre et al. (1996a,b) confirmed that the irregular pulsations of W Vir models are indeed chaotic and they furthermore proved that the physical system generating the time series is equivalent to a system of 3 ordinary differential equations (hereinafter ODEs). A similar approach has been used also for the study of the pulsations of other type of stars like, for instance, the RV Tau stars, R Scuti (Buchler et al. 1995) and AC Her (Kolláth et al. 1998) and has provided significant results concerning the underlying dynamics. This result is not a trivial one since it is not evident at all that stellar pulsations can be fully described by such a simple system of ODEs. This stems from the fact that the classical method to physically describe stellar pulsations is based on the use of a hydrodynamic code where the partial differential equations (PDEs) of fluid dynamics are replaced by a discrete approximation consisting of N mass shells. Therefore, a set of $3N$ coupled nonlinear ODEs must be solved, where N is typically of the order of 60.

From the point of view of the dynamic systems theory, there have been several attempts to interpret the irregularities in the stellar variability from the perspective of chaotic regimes or, equivalently, to discover the nature of the underlying chaotic or intermittent mechanism and how this mechanism produces the observed effects (Buchler & Kolláth, 2001). However, there is no consensus in the literature about which features of the oscillations might be at the root of the chaotic behavior. It is

important to point out here that the observations show that these oscillations become more and more irregular in time, especially at the very end of this evolutionary phase, when the mass loss rate becomes increasingly large. The general approach adopted by most of the studies is to investigate how the outer layers of the stars respond to the pulsations originating in the stellar interior. These outer layers are driven periodically by pressure waves generated well below the stellar photosphere. The outer layers are generally assumed to behave as driven oscillators whose dynamics can be of significant variety: regularly periodic motions, at first, multiperiodic as time increases and, finally, chaotic motions as the mass of the envelope decreases more and more rapidly due to mass loss.

3.1 Description of the one-zone model

In the search for a description which embodies the essentials of stellar oscillations, we follow the simple model of the driven keplerian oscillator extensively studied by Icke et al. (1992) and successfully applied to Asymptotic Giant Branch (AGB) stars. This oscillator has not been used for studying the thermal pulses of Super Asymptotic Giant Branch (SAGB) stars and this is where we concentrate our efforts. The assumptions of the model are the following:

- The outer layers are extended while the interior is compact, and thus the outer layers and the interior are effectively decoupled.
- The driving originates in the stellar interior and consists in a pulsation generated by pressure waves. Moreover, the model considers only the case of sinusoidal driving.
- The outer layers are driven by the interior pressure waves that pass through a transition zone characterized by a certain coefficient of transmission.
- No back reaction of the outer layers is considered on the inner layers.
- The motion is calculated at successive states of hydrostatic equilibrium.

The driving oscillator is generally denominated "the interior" and the driven oscillator, "the mantle". These are separated by a transition zone through which the pressure waves from the interior propagate until they hit the mantle where they dissipate. The driving oscillator is represented by variations of the interior radius, $R_{\rm c}$, around an equilibrium position, R_0, according to:

$$R_{\rm c} = R_0 + \alpha R_0 \sin \omega_{\rm c} t, \tag{3.1}$$

where α is the fractional amplitude of the driving and $\omega_{\rm c}$ is the frequency of the driving (see Figure 3.1). The mantle is represented by a single spherical shell of mass

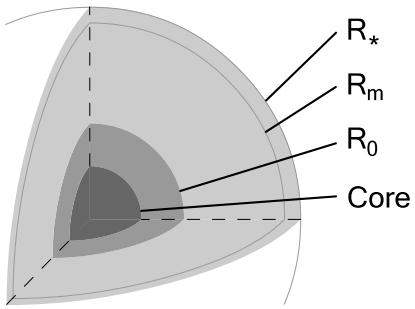

Figure 3.1: Model of the stellar envelope

m at instantaneous radius $R_{\rm m}$. Starting from the equation of motion in the absence of driving force, it can be easily shown that the equation of motion is:

$$\frac{d^2R_{\rm m}}{d\tau^2} = \frac{4\pi R_{\rm m}^2}{m}P - \frac{GM}{R_{\rm m}^2}, \tag{3.2}$$

where τ is the time, P is the pressure inside $R_{\rm m}$, and M is the mass of the rigid core. In accordance with Icke et al. (1992), we additionally assume that the gas follows a polytropic equation of state ($P \propto \rho^\gamma$) with polytropic coefficient $\gamma = 5/3$. If we further assume that the region where the pulsation occurs is nearly isothermal and we focus on the dynamics near the mantle (or, equivalently, that $R_{\rm m} \approx R_\star$, being $R_\star$ the radius of the star), it can be shown that the equation of motion reduces to

$$\frac{d^2r}{dt^2} = -\frac{1}{r^2}\left(1 - \frac{1}{r}\right) + Q\omega^{4/3}\alpha\sin[\omega(t - r + r_0 + \alpha r_0 \sin\omega t)], \tag{3.3}$$

where we have introduced the following set of nondimensional variables:

$$\begin{aligned} r &\equiv R_{\rm m}/R_\star \\ r_0 &\equiv R_0/R_\star \\ \omega &\equiv \omega_{\rm c}/\omega_{\rm m} = r_0^{-3/2} \\ t &\equiv \omega_{\rm m}\tau, \end{aligned} \tag{3.4}$$

where

$$\omega_{\rm m} = \left(\frac{GM}{R_\star^3}\right)^{1/2} \tag{3.5}$$

is the characteristic dynamic frequency of the physical system and Q is the transmission coefficient of the transition zone through which the pressure waves from the interior propagate. In the limit $r \approx 1$ (small oscillations) and absorbing some terms

into t as phase shifts, one arrives to the simplified equation of motion that is the object of the initial part of our study:

$$\frac{d^2x}{dt^2} = -x + \epsilon \sin[\omega(t - x + \alpha\omega^{-2/3} \sin \omega t)], \tag{3.6}$$

where $x \equiv r - 1$ and $\epsilon = Q\omega^{4/3}\alpha$. Note that for $\epsilon = 0$, Eq.(3.6) transforms into the classical equation of the linear oscillator, that is $\ddot{x} = -x$. All the interesting features of the motion are created by the perturbation (the second term of the right-hand side of Eq.(3.6) with $\epsilon \neq 0$) and its interaction with the unperturbed motion ($\ddot{x} = -x$).

The most important parameters of our dynamic system are: α (the fractional amplitude of the driving), ϵ (the total driving amplitude) and ω (which is a measure of the core/envelope ratio, a kind of compactness of the star giving information about where in the interior of the star is the source of the driving). Writing the system as

$$\begin{aligned} \frac{dx}{dt} &= y \\ \frac{dy}{dt} &= -x + \epsilon \sin[\omega(t - x + \alpha\omega^{-2/3} \sin \omega t)], \end{aligned} \tag{3.7}$$

one can see that the system is Hamiltonian, and hence it has the form:

$$\begin{aligned} \frac{dx}{dt} &= +\frac{\partial H(x, y; t)}{\partial y} \\ \frac{dy}{dt} &= -\frac{\partial H(x, y; t)}{\partial x}, \end{aligned} \tag{3.8}$$

where the (time-dependent) Hamiltonian is:

$$H(x, y; t) = \frac{x^2 + y^2}{2} - \frac{\epsilon}{\omega} \cos[\omega(t - x + \alpha\omega^{-2/3} \sin \omega t)]. \tag{3.9}$$

Should the hamiltonian be time-independent (that is, $dH/dt = 0$), then the system would have been also conservative and the Hamiltonian itself or, more precisely, the energy of the system would have been a conserved quantity:

$$\dot{E} = \frac{dH(x, y)}{dt} = \frac{\partial H(x, y)}{\partial x}\dot{x} + \frac{\partial H(x, y)}{\partial y}\dot{y} = 0. \tag{3.10}$$

In our case, the system is hamiltonian, but not conservative ($dH/dt \neq 0$):

$$\frac{dH(x, y; t)}{dt} = \epsilon(1 + \alpha\omega^{-2/3} \cos \omega t) \sin[\omega(t - x + \alpha\omega^{-2/3} \cos \omega t)]. \tag{3.11}$$

It is a well known result of the theory of dynamic systems that in order to do a hamiltonian description of a system, no dissipative processes should be involved in the dynamics. The consequence of this fact is that attractors or repellers do not exist for hamiltonian systems, and therefore one is left with the task of understanding the dynamics of the whole phase space instead of a reduced one. A way to ease this work is to associate a map to the hamiltonian $H(x, y, t)$ and to simplify the visualization of the dynamics. The best choice is the map M represented as $(x_{i+1}, y_{i+1}) = M(x_i, y_i)$, with $i = \overline{1, n}$, where the index i is identified with intervals of t separated by the period of the perturbation, in our case $P = 2\pi/\omega$. This particular stroboscopic map is called the Poincaré map — see Guckenheimer & Holmes (1993) — and constitutes our main analysis tool for this system. It is as well a classical result of the theory of dynamic systems that the Poincaré map of a time periodic hamiltonian system is an *area preserving map* of the plane (Meiss 1992). In fact, this result is the direct consequence of the non-dissipative character of the system. Unfortunately, the fact that the unperturbed motion is linear in nature means that most of the familiar theorems and simplifying tools of the theory of dynamic systems are inapplicable (see Appendix A). This fact gives rise to a rich variety of bifurcations, but it also means that these cases of dynamics are poorly understood. The study of these bifurcations has led us into concluding that the Poincaré map of this system belongs to the family of the so-called *nontwist maps* (del Castillo Negrete et al. 1997). Thus, the transition to the nontwist property as well as to chaos in this area preserving map make the object of this chapter.

3.2 Characterization of the oscillator

For the integration of Eq.(3.6), Icke et al. (1992) used a fourth-order predictor-corrector scheme. Their study was restricted to the following values of the physical parameters: $\epsilon = 0.5,\ 0.75,\ 1.0$, and $\alpha = 0.1,\ 0.2,\ 0.4$ for a small set of values of ω around $\omega \simeq 20$, which is characteristic of regular asymptotic giant branch stars ($M \leq 3\,M_{\odot}$). Their main results and conclusions are that small values of ω produce chaotic pulsations and that for large values of α stable orbits in some definite regions of the phase space are obtained. Our aim is to extend their previous study to SAGB stars, which have, hence, a different value of ω. For the physical conditions found in these stars, $8\,M_{\odot} \leq M \leq 11\,M_{\odot}$ and $R_{*} \sim 450\,R_{\odot}$, it turns out that $\omega \simeq 3$. The exact values for these parameters were obtained from Garcia-Berro et al. (1997). We also intend to further explore the possible range of physical parameters investigated by Icke et al. (1992). For such a purpose we numerically integrate Eq.(3.6) using a fifth order Runge-Kutta integrator with step-size control and dense output (DOPRI5) as described in Hairer et al. (1993). We have used several other integrators, as those described in Shampine & Gordon (1975), which are specifically designed for stiff problems, and we have obtained the same results for a given set of initial conditions (see Appendix B for more details). Thus we conclude that our numerical

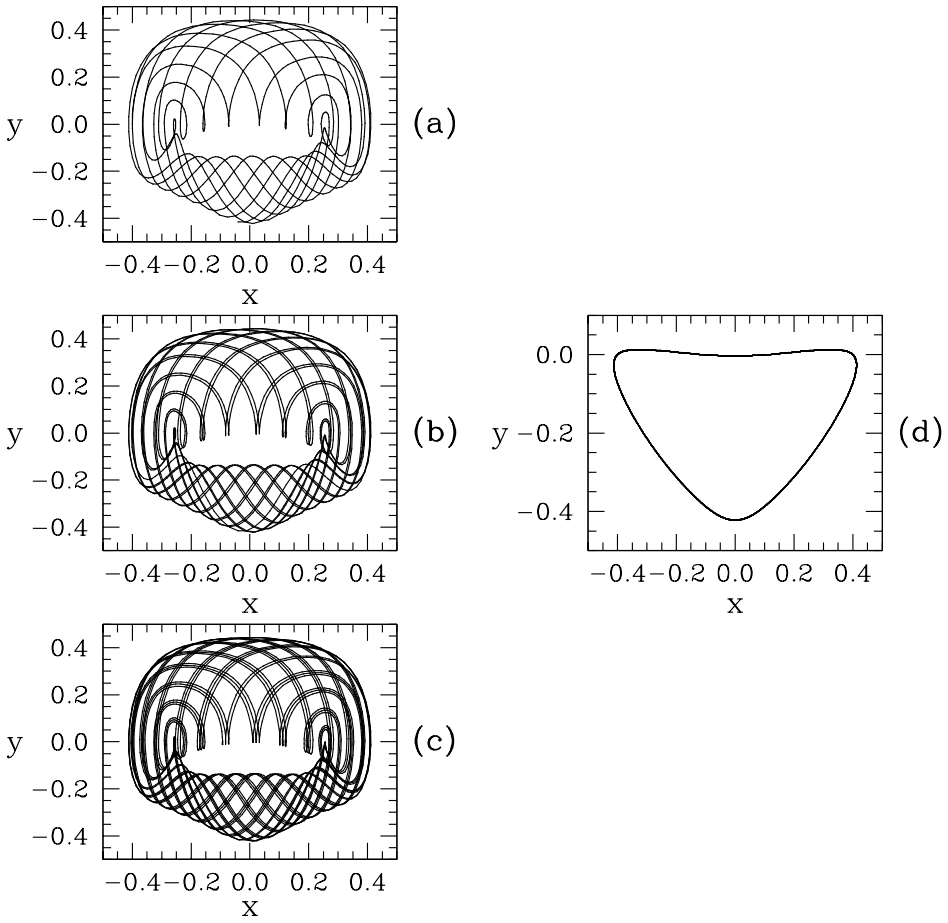

Figure 3.2: Illustration of the quasiperiodic character of the orbit for $\omega = 3.0146$, $\alpha = 0.4$, $\epsilon = 0.5$ and the nondimensional initial condition $(x_0, y_0) = (-0.4, 0.0)$: *(a)* 840 points, *(b)* 1680 points, *(c)* 2520 points, *(d)* Poincaré map of the orbit.

integrator is appropriate for the kind of problem we are dealing with.

3.2.1 AGB stars vs. SAGB stars: the role of ω

We expect that for the physical conditions of SAGB stars these time series should show either a periodic behavior, or quasi-periodic oscillations or even they could show chaotic variability as is the case of regular AGB stars. Generally speaking, a quasiperiodic orbit can be better visualized on the surface of a torus or in a section-cut of this torus, that is in the Poincaré map. However, sometimes a direct image of the orbits given by the numerical integration can help in visualizing how the orbits fold due to the quasi-periodicities. In order to better understand this concept, both

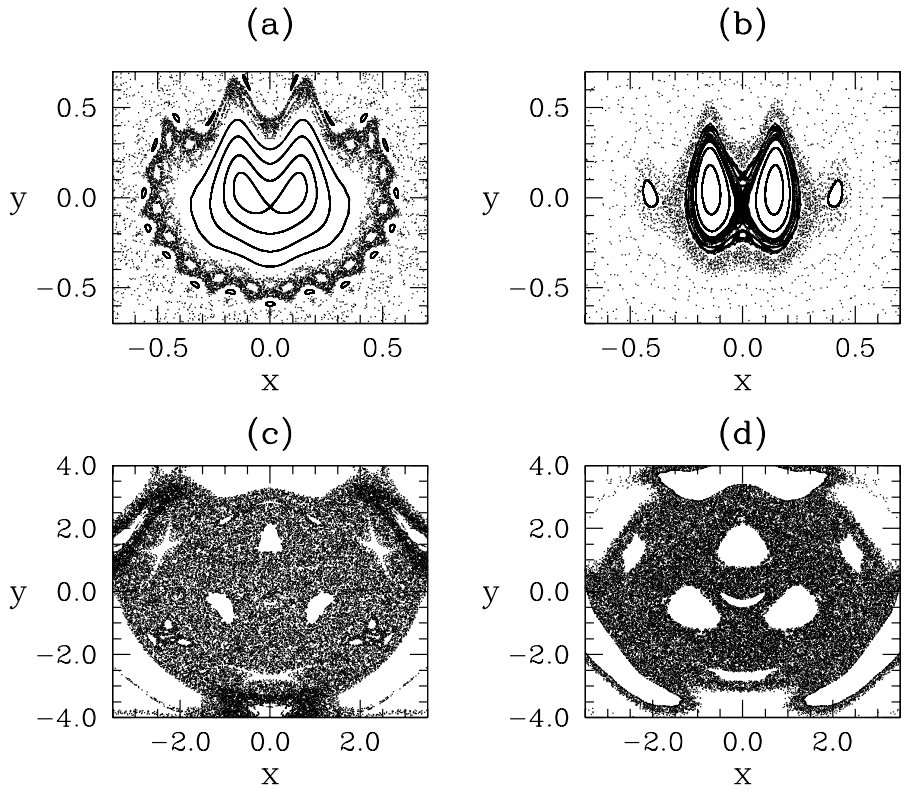

Figure 3.3: Poincaré map for Eq.(3.6) with $\epsilon = 1$ and several initial conditions for $\omega = 20.1$: *(a)* $\alpha = 0.1$; *(b)* $\alpha = 0.4$, and for $\omega \simeq 3$: *(c)* $\alpha = 0.1$; *(d)* $\alpha = 0.4$. Note the difference in the scales of the axes.

a real orbit and its Poincaré map are shown in Figure 3.2, for $\omega \simeq 3$. In particular, considering a time interval equal to an arbitrary integer multiplier, m, of the main period, $P = 2\pi/\omega$, panels (a), (b) and (c) of Figure 3.2 show an orbit for the time intervals $[0, mP]$, $[0, 2mP]$ and $[0, 3mP]$, respectively, with a time interval of $P/30$ between successive points whereas panel (d) shows its corresponding Poincaré map (that is, with P).

In order to compare the behavior for two different values of ω (and, thus, the difference between the behavior of the pulsations of Asymptotic and Super-Asymptotic Giant Branch stars), in panels (a) and (b) of Figure 3.3 we show two Poincaré maps, obtained with different initial conditions and $\omega \simeq 20$, typical of regular AGB stars, whereas in panels (c) and (d) of Figure 3.3 the corresponding Poincaré maps for $\omega \simeq 3$ (typical of SAGB stars) and the same initial conditions are shown. As it can be seen in this figure, as ω increases the behavior is more irregular, and the islands and the structure of panels (a) and (b) quickly disappear, leading to a more chaotic behavior. Consequently we expect to find a more chaotic behavior for the pulsations of SAGB stars. As time-series are the main object of study in astronomy, we illustrate in Figure 3.4 the time series for the velocity variations of some initial conditions (x_0, y_0) of the Poincaré map of panel (b) of Figure 3.3, while the corresponding time

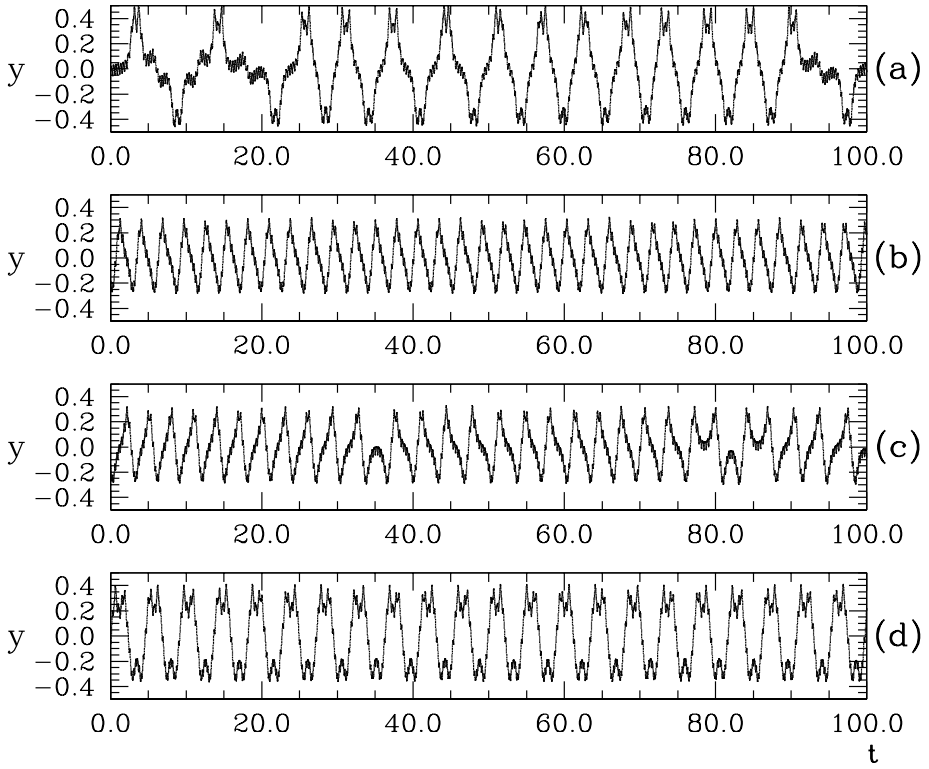

Figure 3.4: Velocity variations corresponding to $\epsilon = 1$, $\alpha = 0.4$, $\omega \simeq 20$ and several initial combinations of (x_0, y_0): *(a):* $(-0.35, -0.05)$, *(b):* $(-0.1, -0.2)$, *(c):* $(0.2, -0.15)$, and *(d):* $(-0.25, -0.05)$.

series for the case of panel (d) are shown in Figure 3.5. Note however, the different scales involved in Figure 3.3, which translate into larger periods for Figure 3.5, when compared to Figure 3.4.

As we have seen so far, the Poincaré map of our system looks quite bizarre, and consists in domains of chaotic orbits, in islands (i.e. closed curves) filled with periodic and quasiperiodic orbits and in smaller domains where chaos exists. In fact, this system shows several good examples of the topological zoo typical of hamiltonian systems. The existence of islands was generally regarded as irrelevant in determining the origin and character of chaos in hamiltonian systems (Zaslavsky 1999). However, thorough analysis of this issue has shown that the behavior near the boundaries of such islands is very interesting. In particular, crossing an island boundary means jumping from a regular (periodic or quasiperiodic) behavior to an irregular one that lies in the chaotic region (or stochastic sea, as it is generally called). One of the particularities of this singular zone is illustrated in Figure 3.3a. One can see a central island embedded in the domain of chaotic motion with an interesting boundary separating the area of chaos from the one of the regular motion. By changing a control parameter of the system, numerous bifurcations are born and thus influence the topology

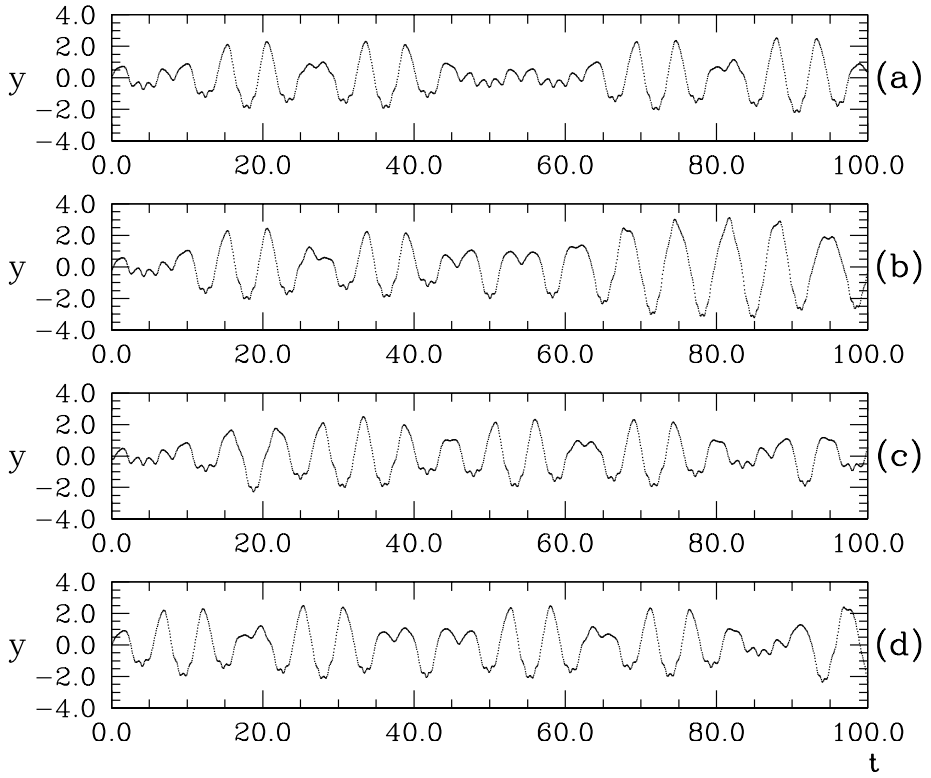

Figure 3.5: Velocity variations corresponding to $\epsilon = 1$, $\alpha = 0.4$, $\omega \simeq 3$ and several initial combinations of (x_0, y_0): *(a):* $(-0.35, -0.05)$, *(b):* $(-0.1, -0.2)$, *(c):* $(0.2, -0.15)$, and *(d):* $(-0.25, -0.05)$.

of the boundary zone leading to the appearance and disappearance of smaller and smaller islands. It may result in self-similar hierarchical structures of islands which is crucial for understanding long-term behavior and interpreting the spectrum analysis of the time-series as these structures represent high-order resonances.

3.2.2 The role of the fractional driving amplitude, α

In order to characterize in depth the behavior of our system, we have performed a thorough parametric study by varying α and ϵ, while keeping ω constant at the value typical of SAGB stars. Reasonable values of the fractional amplitude, α are in the interval 0.1–0.4, whereas the total driving amplitude, ϵ varies between 0.1 and 1.0. Since α is the ratio between the amplitude of the internal driving and the radius of the star, the upper limit considered in this study is 40%, which is physically sound. In general, a star is characterized by its compactness (ω) and the interior-mantle coupling strength (Q). Accordingly, we have investigated the dynamics of the solution of Eq.(3.6) rewritten below in the form of a perturbed oscillator,

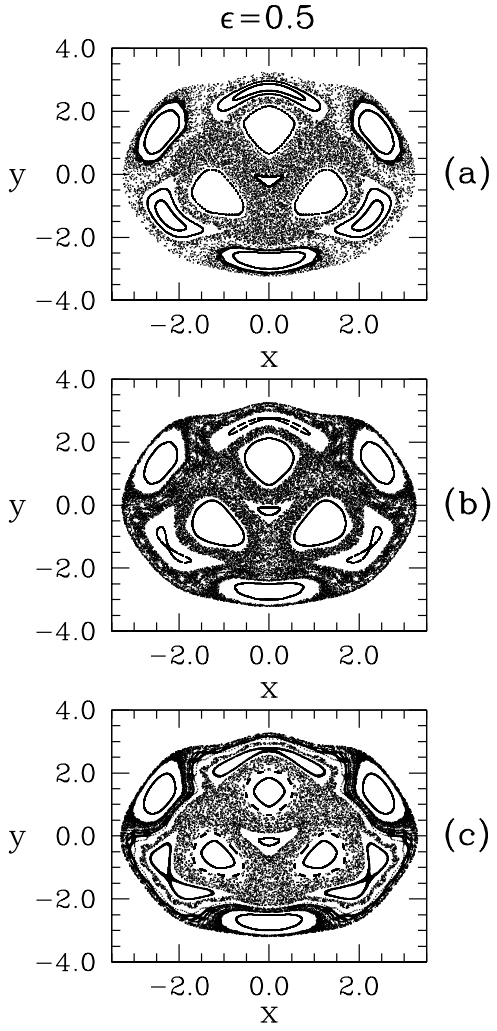

Figure 3.6: The effect on the Poincaré map of increasing α: *(a)* $\alpha = 0.2$; *(b)* $\alpha = 0.3$ and *(c)* $\alpha = 0.4$.

$$\ddot{x} + x = \epsilon \sin[\omega(t - x + b \sin \omega t)], \tag{3.12}$$

where $b = \alpha\omega^{-2/3}$, maintaining a constant value of $\omega \simeq 3$ and varying ϵ (and implicitly Q). The Poincaré map was used to study the general behavior of the system in Eq.(3.6).

In a first step, we have studied the qualitative changes in the dynamics (that is, the bifurcations) as the parameters ϵ and α are varied. We have considered the case $\alpha \in (0.1, 0.4)$ and $\epsilon = 0.5$, and we have obtained, starting from several initial conditions, the Poincaré maps of our system corresponding to these parameters (Figure 3.6). The Poincaré maps are characterized by the same geometric structure: a region, centered

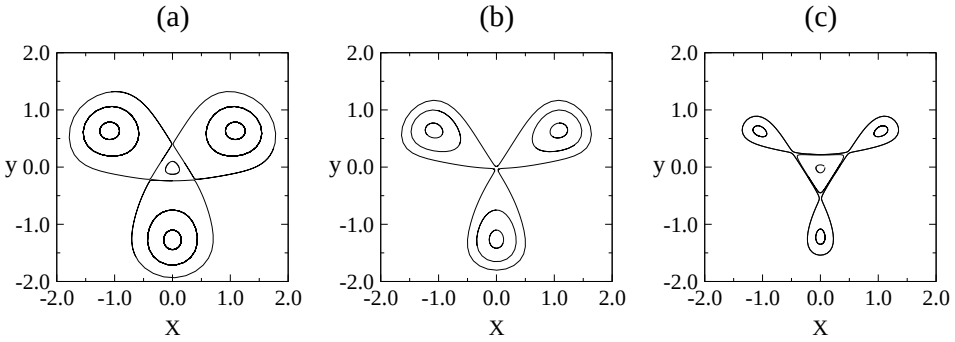

Figure 3.7: The behavior of the central elliptic fixed point for our area preserving map for $\omega = 3.0146$ and $\epsilon = 0.07$. *(a):* $\alpha = -0.3$; *(b):* $\alpha = -0.05$; *(c):* $\alpha = 0.2$

around $(x, y) = (0, 0)$, of closed orbits, surrounded by a region of chaotic orbits. As it can be seen in Figure 3.6, as α increases, the central region of regular behavior expands to the detriment of the stochastic sea.

We also have paid some attention to the behavior of the system for *negative* values of the parameter α. A quick look at Eq.(3.1) allows one to see that negative values of α correspond to a mere change of phase in the driving and, therefore, they also correspond to physically meaningful cases. However, and for the sake of clarity and conciseness, along this study we will concentrate our efforts on the positive domain of this parameter. However, we would like to remark at this point that the phase portrait of the Poincaré map changes drastically depending on whether α is positive, negative or almost zero (Figure 3.7).

3.2.3 The role of the total driving amplitude, ϵ

Next we have focused on values of $\epsilon \ll 1$ in order to observe in detail the departure of our equation from the harmonic oscillator as this parameter is increased. We restricted the study of the Poincaré map to a rectangle limited by initial conditions close to reasonable values of the radius and velocity of the mantle. The restriction is also due to the approximations involved in reaching Eq.(3.6). For $\epsilon = 0$ we get an integrable hamiltonian system, whose integrals of motion are the tori given by the condition $x^2 + y^2 = C,\ t = [0, 2\pi/\omega)$. The Poincaré map has the elliptic fixed point (0, 0), which corresponds to a periodic orbit of period $P = 2\pi/\omega$ of the perturbed hamiltonian system.

We have chosen the range of $\epsilon \in (0, 0.12)$ and $\alpha = 0.3$ and obtained a cascade of bifurcations in the form of chains of alternating elliptic and hyperbolic points, with regular curves encircling the elliptic fixed points and a separatrix connecting the hyperbolic points (Figure 3.8). From the general theory of nontwist maps, it results that for a given ϵ, there exists a critical value of α, which depends on ϵ, for which the elliptic fixed point undergoes a type of bifurcation called triplication (Dullin et al., 2000). Figure 3.8 illustrates the route to triplication. The upper panels correspond

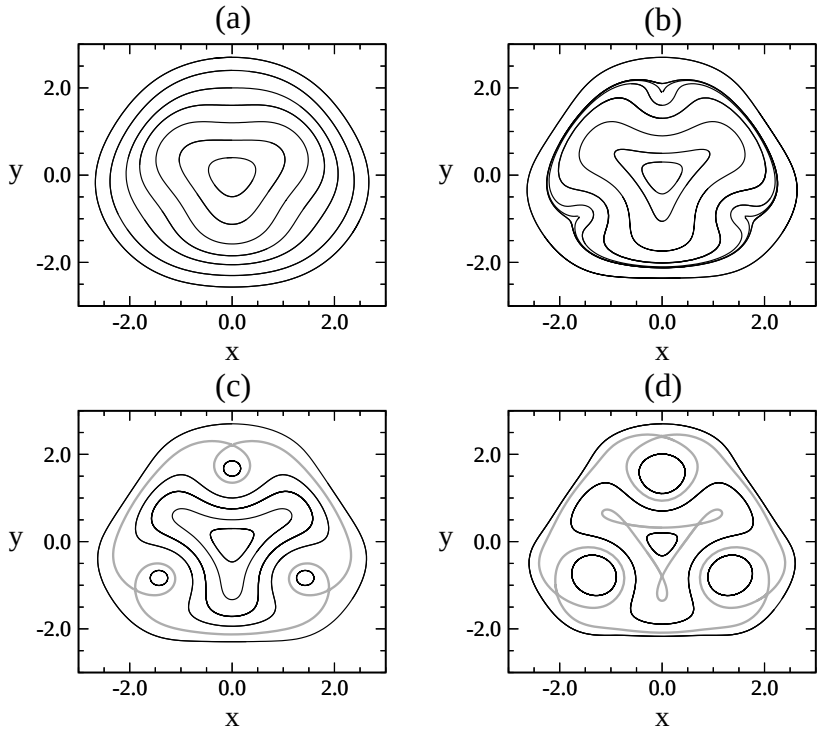

Figure 3.8: Poincaré maps for Eq.(3.12) for $\alpha = 0.3$ and different values of ϵ: *(a)* $\epsilon = 0.01$ — an "almost" harmonic oscillator; *(b)* $\epsilon = 0.03$ — the phase portrait just before the saddle-center bifurcation; *(c)* $\epsilon = 0.04$ — the creation of the first dimerized island chain; *(d)* $\epsilon = 0.07$ — the pair of period–3 dimerized island chain is complete. The separatrices responsible for the creation of chaotic behavior appear in light-grey.

to values of ϵ for which $\alpha = 0.3$ is smaller than the critical value. For these cases the elliptic point has not yet undergone a triplication, but it is at the threshold of creation of a three-periodic island (one can see an invariant circle with three cusps). This is a stage in the typical scenario of creation of new type of orbits in nontwist maps. The bottom panels of Figure 3.8 correspond to configurations typical of a parameter α greater than the threshold of bifurcation. The transition from the phase-space of the top-left panel to the one in the bottom-left panel through the cusp phase of the top-right panel is a typical case of *saddle-center (cusp) bifurcation* (Iooss & Joseph, 1990). Each cusp from Figure 3.8*b* is a point of a new periodic orbit created through a saddle-center bifurcation for $\epsilon \approx 0.04$: a stable (elliptic) and an unstable (hyperbolic) fixed point emanate from each cusp (see Appendix A). The homoclinic loop of every hyperbolic point surrounds the corresponding elliptic one. Between two successive hyperbolic points (in cyclic order) there is a heteroclinic connection. These separatrices that appear in grey in Figure 3.8*c,d* are called dimerized island chains (del Castillo Negrete et al., 1996). With the formation of the second dimerized chain, the scenario is said to be complete, in the sense that two chains of the same

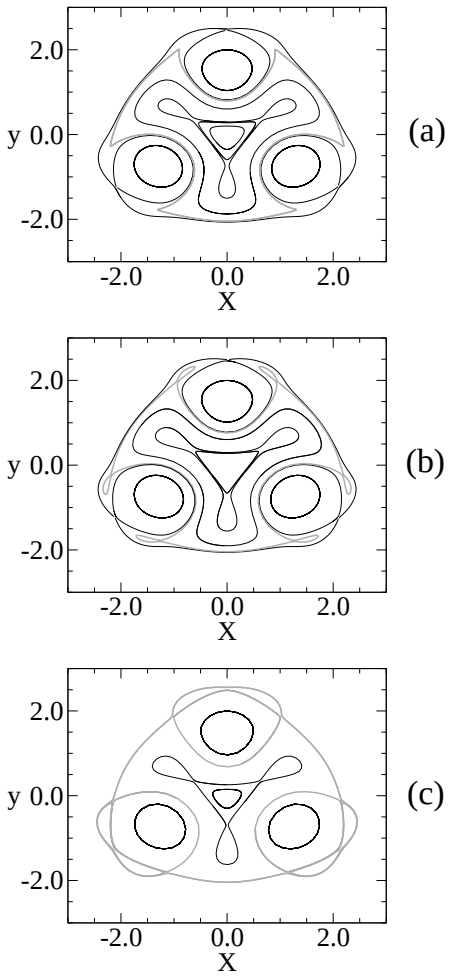

Figure 3.9: The global bifurcation: creation by saddle-center bifurcations of a pair of period–3 orbits for $\alpha = 0.3$ and increasing values of ϵ. The particular orbits involved in the bifurcations appear in light-grey. *(a)* $\epsilon = 0.0875$ — the phase portrait at the threshold of a saddle-center bifurcation. It presents an invariant curve with six cusps; *(b)* $\epsilon = 0.095$ — two interwined orbits of period–3 have been created. Inside each new-born loop there is a period–3 elliptic point; *(c)* $\epsilon = 0.11725$ — the threshold of the global bifurcation. The topology of the separatrices has changed.

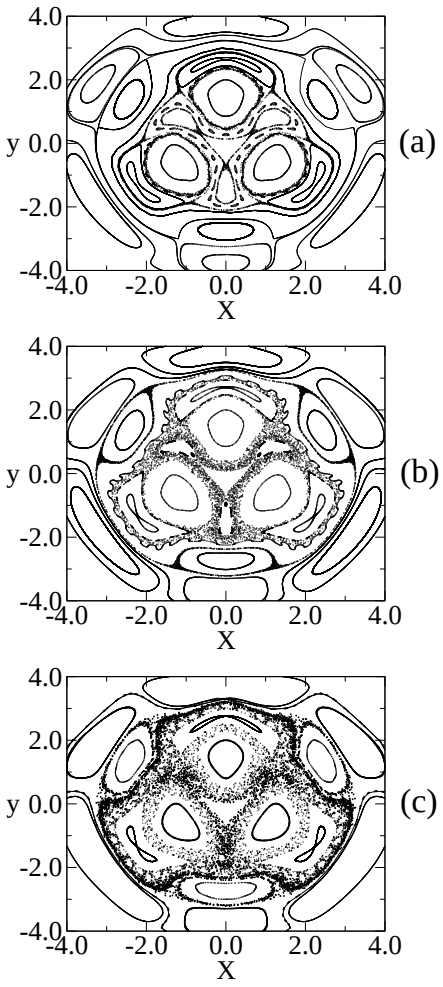

Figure 3.10: Formation of the stochastic sea($\alpha = 0.3$): *(a)* $\epsilon = 0.3$ — as the second dimerized island chain is destroyed, it is clothed in a stochastic layer; *(b)* $\epsilon = 0.4$ — the stronger the perturbation, the wider the stochastic layers; *(c)* $\epsilon = 0.5$ — merging of the stochastic layers forming the stochastic sea.

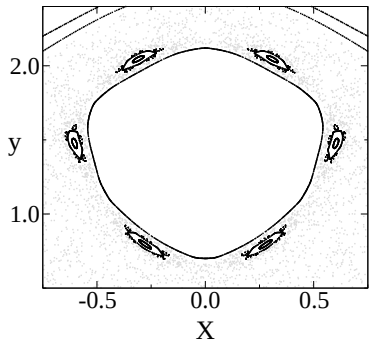

Figure 3.11: A zoom of Figure 3.10*c* illustrating the islands-around-islands hierarchy.

type appear in stages, forming a sequence of vortices (Van der Weele & Valkering 1990).

Around the configuration typical for a step of the triplication, a sequence of local and global bifurcations occurs. This is illustrated in Figure 3.9, where it can be seen that two independent orbits of the same period three are created by cusp bifurcation. They evolve in such a way that, finally, they interact with the orbits which belong to the first dimerized island chain. As ϵ increases the newly born elliptic points approaches the hyperbolic points of the dimerized chain. When ϵ reaches a value of about 0.11725 a global bifurcation occurs: the newly created orbits interfere, and the hyperbolic points of the dimerized island become homoclinic eight-like orbits encircling the new created elliptic points. If we enlarge the region of study of the Poincaré map we can observe that as ϵ increases the process of creation of vortices repeats. In § 2.6, dedicated to the mathematical details of the model, we shall argue that this behavior is due to the oscillating character of the nontwist property of perturbation.

In a second step we have paid attention to larger values of ϵ. In particular we have studied the range $\epsilon \in (0.2, 0.5)$. The increase in strength of the external perturbation destroys these separatrices (Figure 3.10*a*) by clothing every one of them in a stochastic layer (Figure 3.10*b*). As the thickness of the layers increases with the perturbation, depending on the positions of the separatrices in the phase space, they can merge forming the stochastic sea (Figure 3.10*c*). Any trajectory whose initial condition belongs to the stochastic sea passes through every point of the sea. Thus, the entire sea can be explored with the help of a single trajectory.

Another essential phenomenon typical of some hamiltonian systems is linked to the existence of a very complex phase space topology in the neighborhood of some islands: a trajectory can spend an indefinitely long time in the boundary layer of the island. Therefore, these regions are called *dynamical traps* (Zaslavsky, 2002). This trapping phenomenon was observed already in Contopoulos (1971) and was later called *stickiness* (Shirts & Reinhardt, 1982). The main uncertainty in characterizing this phenomenon concerns the level of stickiness (that is, its characteristic trapping time) which depends on the parameters of the system in a still unknown manner. In

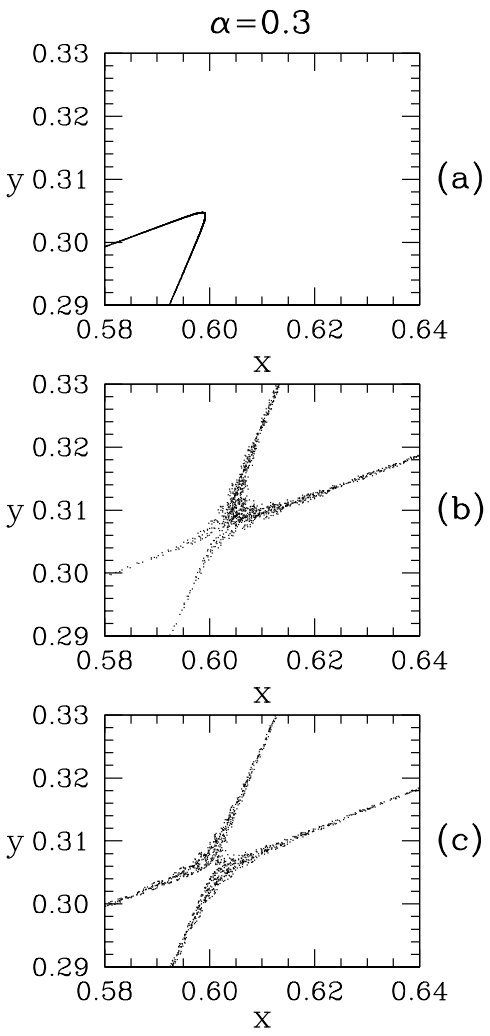

Figure 3.12: The evolution in time of the initial condition $(x_0, y_0) = (0.0, 0.2)$ as ϵ is increased for $\alpha = 0.3$: *(a)* $\epsilon = 0.190175$: *(b)* $\epsilon = 0.190185$, and *(c)* $\epsilon = 0.190192$. The initial condition is $(x_0, y_0) = (0.0, 0.2)$.

general, close to the islands there is a hierarchical structure of islands-around-islands whose presence is believed to explain the origin of the stickiness of the trajectory within this region, and is the reason why this behavior is called *hierarchical-islands trap* (Figure 3.11). The reason why so much attention is generally paid to understanding the structure of these islands is because different islands may correspond to different physical processes responsible for their origin. An island in the stochastic sea refers to the domain of initial conditions that generate stable trajectories. Its boundary layer may include higher-order resonant islands. A more important reason is that the topology of the islands could be an indicator for the vicinity of bifur-

cations. However, no general description for the birth and collapse of hierarchical islands exists yet.

A zoom of the region near one of the hyperbolic points reveals that the seed of chaos already exists (Figure 3.12) even before the destabilization of the separatrix followed by the creation of the stochastic layer — see also Lieberman & Lichtenberg (1992). There are numerous islands which the chaotic trajectory cannot penetrate. Within an island there are regions of quasiperiodic motion (invariant tori) and regions of trapped chaos. The stronger the chaos is, the smaller the islands are and the larger is the fraction of phase space occupied by the stochastic sea. The coexistence of regions of regular dynamics (closed orbits) and regions of chaos in the phase space is a wonderful example of the property which differentiates chaotic systems from ordinary random processes, where no stability islands are present. This property makes possible the analysis of the onset of chaos and the appearance of minimal regions of chaos. To summarize the dynamic behavior as it results from Figure 3.8 and Figure 3.9:

(a) For $\epsilon \in [0, 0.03)$, the Poincaré map is similar to that of the harmonic oscillator, with the elliptic fixed point in $(x, y) = (0, 0)$ surrounded by almost circular closed orbits.
(b) For $\epsilon \in [0.03, 0.04)$, in addition to the central elliptic point, three elliptic and three hyperbolic fixed points appear, all of period 3, together with the associated heteroclinic orbit that connects them.
(c) For $\epsilon \in [0.04, 0.07)$, appear new fixed points, three of them are elliptic and three are hyperbolic of period 3 connected by a second heteroclinic orbit (inside the first heteroclinic orbit).
(d) For $\epsilon \in [0.07, 0.2)$, the first heteroclinic orbit disappears and three homoclinic orbits of period 3 are created, each of them implying the existence of two elliptic fixed points and a hyperbolic one. The elliptic fixed points are created at this step while the hyperbolic ones were those created at step (c).
(e) For $\epsilon \in [0.2, 0.3)$, we notice a more definite chaotic behavior created by the instability of the remaining of the first heteroclinic orbit engulfing the fixed points of case (c).
(f) For $\epsilon \in [0.3, 0.5]$, we notice the extension of the chaotic orbits in the central region (without altering the Poincaré map), together with the continuous generation of pairs of three elliptic fixed points in the outer region as ϵ increases.

Another important feature of the phase portrait characteristic of nontwist maps is the existence of *meanders*, i.e. invariant circles which fold exactly as a meander (Simó, 1998). Meanders are created between two successively born dimerized island chains or between two chains of vortices. Panel a of Figure 3.13 illustrates a meander near a pair of dimerized island chains containing periodic orbits of period 35. Meanders appear to be robust invariant circles, even when the nearby orbits are chaotic (Figure 3.13*b*). This behavior was observed in nontwist standard-like maps, but until now there is no explanation for this robustness.

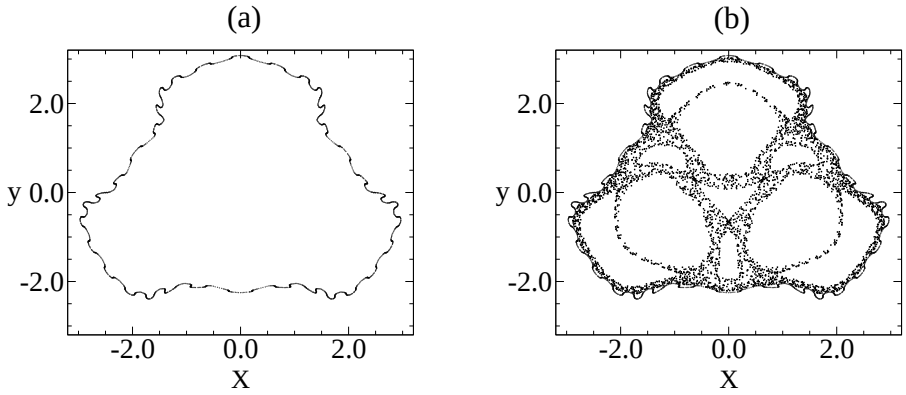

Figure 3.13: *(a):* A meander near an invariant circle with 35 cusps for $\epsilon = 0.4$ and $\alpha = 0.3$; *(b):* two orbits, one filling the meander and the second, a chaotic orbit. The meander confines the chaotic orbit.

3.3 Astrophysical interpretation of the results

In order to give an idea of the physical ranges for the stellar fluctuations in radius and velocity and for an ulterior comparison with light curves obtained from observational data, we discuss below some time series obtained with the model presented above that we consider to be of interest. Also, and for physical purposes, the variations of radius and of the velocity as functions of time are represented both in physical units (years, solar radii and km/s, respectively) and in nondimensional units — as we have been doing so far. For instance, in Figure 3.14 we show the time series $(R(\tau), V(\tau))$ corresponding to the quasiperiodic Poincaré map of Figure 3.2 in physical coordinates.

Generally speaking, the primary information that one can derive from a generic computed or observed time series is the spectral distribution of energies (or amplitudes) of the light curve, that is the amplitudes and periods present in its Fourier spectrum. Very frequently, these time series do not show a single frequency or a small set of frequencies but, in addition, linear combinations of these primary frequencies may also appear in the spectra. A good example of this — among many others — is the Cepheid TU Cassiopeia (Kolláth & Buchler, 2001) for which 29 frequencies have been identified. Even terms like $4f_0 + 3f_1$ or $5f_0 + 2f_1$ are inferred from the Fourier transform of the light curve. In sharp contrast, in the spectra of RR Lyrae typically only the $f_0 \pm f_1$ terms can be identified in addition to f_0 and f_1. The Fourier spectrum of the velocity variation of Figure 3.14 is shown in Figure 3.15 together with the representation of linear combinations of the two basic frequencies $f_0 = 0.5227$ yr^{-1} with A_0=0.32 km/s and $f_1 = 0.8501\ yr^{-1}$ with A_1=11.95 km/s. As it can be seen in this figure there are several linear combinations of the two basic frequencies. In particular the most characteristic combinations are $f_0 + f_1$, $f_0 + 2f_1$, $f_0 + 3f_1$ and $f_0 + 4f_1$, but other linear combinations are already quite apparent.

In any calculation of a time-varying phenomenon, like the one we are studying

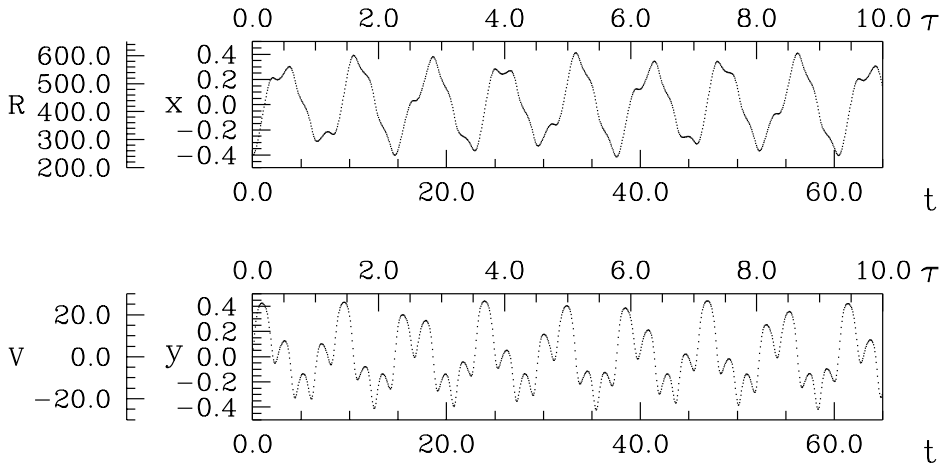

Figure 3.14: Time series for the quasiperiodic orbit previously shown in Figure 3.2. The variations of the radius *(top)* and of the velocity *(bottom)* are shown as a function of time (τ in years and t nondimensional), expressed both in nondimensional units and in physical units (solar radii for the radius, km/s for the velocity).

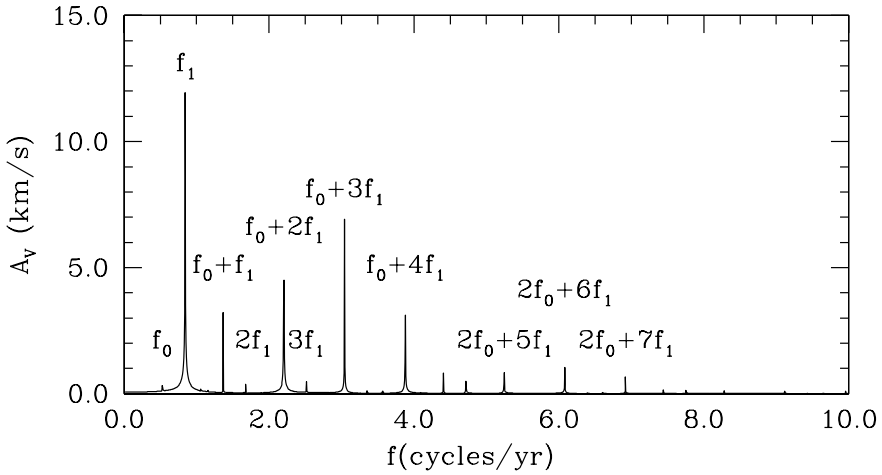

Figure 3.15: Fourier spectra for the velocity variation of Figure 3.14.

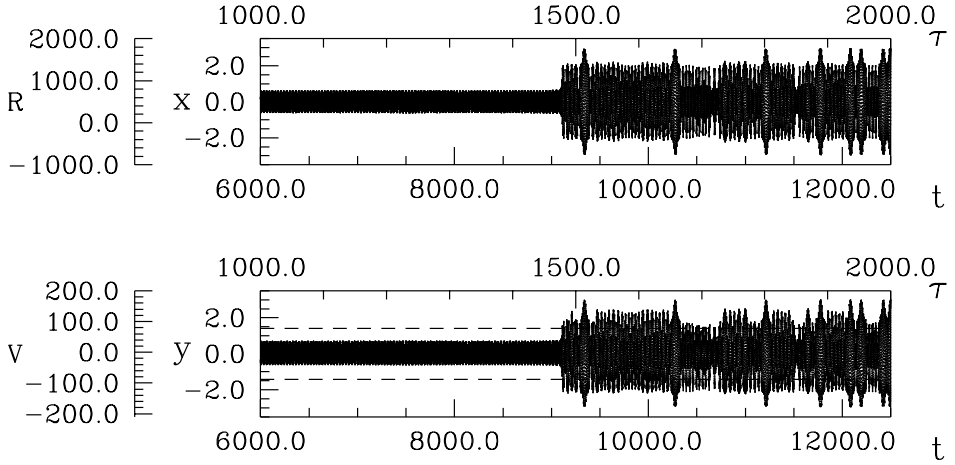

Figure 3.16: Variations of radius *(top)* and velocity *(bottom)* as a function of time for $\omega \simeq 3$, $\alpha = 0.3$, $\epsilon = 0.5$ and the initial condition $(x_0, y_0) = (0.0, 0.02)$. The escape velocity of the model star ($v_{\rm esc} \simeq 86$ km/s) is represented as a dashed line.

here, there is always the very important practical question of when the simulations should be terminated. For full nonlinear hydrodynamic simulations, even in the case in which a stable limit cycle seems to have set in, one often is worried about the fact that thermal changes, which take place on a longer timescales, could still be occurring. For instance, Ya'ari & Tuchman (1996) have carried the calculations of Mira variable pulsations much further than in previous investigations and, to their surprise, they have found that the actual behavior was significantly different from what it was previously thought. To be precise, they obtained a new modified "true" limit cycle which is quite different from the earlier, "false", limit cycle. In agreement with these results, the numerical integration of our system, despite the very crude approach adopted here which results in an extreme simplicity of the model, presents a similar behavior. This is shown in Figure 3.16 for a particular orbit. As it can be seen in this figure during the first ~ 1400 yr the star oscillates quite regularly, and with small amplitudes. After this period of time the quiet phase suddenly stops and the pulsations become more violent and irregular. Moreover, at late times the velocity of the outer layers reaches values which are in excess of the escape velocity (which is represented in the bottom panel of Figure 3.16 by a dashed line) and, hence, mass loss is very likely to occur, in accordance with the observations of LPVs, which are the observational counterparts of SAGB stars.

This behavior — a quiet phase, followed by an extremely violent phase — is a typical case of a dynamic trap discussed in §3.2. The Poincaré map associated to the radius and velocity variations in Figure 3.16 is shown in Figure 3.17. Neither Figure 3.16 nor Figure 3.17 include the oscillations previous to 1000 years because the behavior is similar to the one of the time interval between 1000 and 1400 years and, thus, was excluded from the figures in order to have a better view of the time series.